Journal of Hydrology 609 (2022) 127760

Contents lists available at ScienceDirect

Journal of Hydrology

journal homepage: www.elsevier.com/locate/jhydrol

Research papers

Assessing irrigation mitigating drought impacts on crop yields with an integrated modeling framework

Proloy Deb [a,b,*], Hamid Moradkhani [a,b], Xiaoliang Han [a,b], Peyman Abbaszadeh [a,b], Lei Xu [a,b]

[a] Center for Complex Hydrosystems Research, The University of Alabama, AL 35487, USA
[b] Department of Civil, Construction and Environmental Engineering, The University of Alabama, Tuscaloosa, AL 35487, USA

ARTICLE INFO

Keywords:
Droughts
CROPWAT
AquaCrop-GIS
Mobile River Basin
Corn
Soybean

ABSTRACT

Irrigation is one of the major adaptation strategies to combat the negative impacts of drought on crop yields. However, during droughts, the water resources are limited and determining the exact irrigation amount and its response to crop yields are crucial. Existing crop yield simulation models are data-intensive and a majority of these are point-based. Therefore, this study presents a novel integrated modeling framework by using two parsimonious models (CROPWAT, an irrigation water requirement simulation model; and AquaCrop-GIS, a spatial crop yield simulation model) to simulate corn and soybean yields under different irrigation application rates during drought years at a spatial scale in the Mobile River Basin (MRB), Southeast U.S. To simulate crop yields for drought years, first agricultural drought years are identified using an integrated drought index called the Standardized Precipitation Evapotranspiration Soil Moisture Index (SPESMI). The results indicate that a majority of the basin was affected by mild to extreme droughts during the years 2008, 2011, 2012, 2016. The results of the integrated modeling framework illustrate the potential corn and soybean yields can be increased from 10% to 259% and 20% to 229% respectively under different irrigation water application rates (50%, 75%, and 100% of irrigation water requirement) relative to rainfed crop yields at the counties in the MRB during drought years. These findings demonstrate the importance of overall irrigation and the integrated modeling framework in devising robust irrigation water management plans in drought-affected areas at a spatial scale. Failure in integrating irrigation water requirement models in crop yield simulations will result in erroneous yield simulations, especially during droughts – this is salient given projections for frequent and intense droughts globally. Although the study is focused on MRB, the framework developed is applicable for irrigation planners and water managers in any region that experiences mild to extreme droughts, as long as the farmers have the ability to adapt the irrigation in their practice given socio-economic constraints.

1. Introduction

Drought is a natural phenomenon characterized with below-normal water availability and can occur in any region across the world (Van Loon et al., 2016). Severe and prolonged droughts can have serious implications in agriculture and may result in significant crop yield reductions posing a serious threat to food security (Hameed et al., 2020; Park et al., 2016). According to a global study by Kim et al. (2019) during the drought period of 1983 – 2009, 75% of the harvested areas have experienced crop yield loss with an estimated value of 166 billion US dollars. Additionally, Lesk et al. (2016) showed in a global study that cereal production was reduced by 9 – 10% due to high temperature and droughts during the period of 1964 – 2007. In another study in the United States (US), corn (*Zea mays*) and soybean (*Glycine* max) yields were found to be highly correlated with the Standardized Precipitation Evapotranspiration Index (SPEI), with significant yield reductions during intense drought periods (Peña-Gallardo et al., 2019). Similarly, Zipper et al. (2016) analyzed US corn and soybean yield sensitivity to meteorological drought from 1958 to 2007 and concluded that overall droughts resulted in to 13% in crop yield variability, especially the southeastern region which was becoming more sensitive over time. Furthermore, Ray et al. (2018) identified that droughts negatively impacted not only crop yield, but also cultivated areas (hectarage) in Texas, US where the cotton and corn hectarage declined to 21% and 18% respectively during drought years (2011 – 2013) compared to 30 year average crop hectarage. These negative impacts of droughts on

* Corresponding author at: Center for Complex Hydrosystems Research, The University of Alabama, AL 35487, USA.
E-mail address: pdeb1@ua.edu (P. Deb).

https://doi.org/10.1016/j.jhydrol.2022.127760
Received 7 July 2021; Received in revised form 15 March 2022; Accepted 20 March 2022
Available online 25 March 2022

agricultural production have raised serious concerns regarding food security among the science and research community (Kim et al., 2019; Yu et al., 2018).

Irrigation is an effective adaptation practice that supplements the additional water (unmet from precipitation) required by crops. Globally, the irrigated areas have roughly doubled in the last five decades and contributed to a significantly increase in crop yields (Foley et al., 2011). Global land use based classification studies have confirmed that irrigated croplands account for 25% of the global cropped area, yet it contributes to 43% of the global crop production (Portmann et al., 2010; Siebert and Döll, 2010). A worldwide study on 26 crops reported that if all the rainfed croplands were converted into irrigated lands, the global crop production might rise by 20% under the current climate (Siebert and Döll, 2010). Climate change projection studies have estimated the global irrigated croplands in the future to range from 240 to 800 Mha in 2050 (Alexandratos and Bruinsma, 2012; Puy et al., 2020), and in the range of 4.5 – 21.9 Mha alone in the US by 2090 (McDonald et al., 2013). Although these are either country-scale or global studies, at state scales these projection values are different. For instance, in Alabama, Georgia, and Mississippi the rate of increase in the irrigated area is significantly lower than the major cropping belts in the US (Abbaszadeh et al., 2022; Gavahi et al., 2021; Schaible and Aillery, 2012). There are several factors contributing to this, but two major causes are: (1) the existence of riparian water rights in Alabama and restriction in water use in Georgia (100,000 gallons/day), and (2) high capital investment in irrigation equipment and lack of incentives from the government (Hollis, 2011).

Several drought indices are developed across the US, a few of them focusing on the southeast region. Specifically *AgClimate* (now AgroClimate), a climate forecast information system for agricultural risk management (Fraisse et al., 2006) comprises of Agricultural Reference Index for Drought, a drought index for estimating the water stress affecting crop growth (Woli et al., 2012). Additionally, the US Drought monitor and the Palmer Drought Severity Index (PDSI) were also specifically developed in the US. All of these indices indicate that the southeast US region has experienced intense and frequent droughts in the past and recently (as per US drought monitor in 2012 extreme to exceptional drought and in 2018 severe to extreme drought during cropping seasons) Gavahi et al. (2020) also highlighted the same. Since, droughts are identified to have a negative influence on corn and soybean yields in the US, specifically during the crop development periods (Zipper et al., 2016), the states in the southeast US plan to intensify irrigation in the future to avoid crop yield loss. Furthermore, climate projection studies in the region suggest shortages of freshwater (Boretti and Rosa, 2019; Sun et al., 2013). Therefore, judicious use of irrigation water at regional scale (at county level) is critical for achieving the potential yield and regional food security, especially during droughts (Evans and Sadler, 2008).

While numerical modeling is an approach to calculating optimal irrigation amount and assessing yields, the existing modeling studies are limited to stand-alone application of irrigation water requirement (IWR) estimation models for calculating irrigation amounts, and irrigation scheduling (He et al., 2013; Mason et al., 2019). Additionally, the existing crop yield model simulation studies are limited to simulating crop yield based on user-defined IWR (Kephe et al., 2021; Mubeen et al., 2020; Yu et al., 2018). Simulating IWR separately and then forcing these into a crop yield simulation model is a two-step process and is tedious. Although, there is a gridded crop model intercomparison simulation dataset, which comprises global crop yield data under both rainfed and irrigated conditions (Müller et al., 2019), the spatial resolution of the dataset is too coarse (0.5 arc-degree ~55 km) which limits its application in regional planning and management (Kim et al., 2021). On the other hand, a plethora of existing IWR and crop yield simulation studies are generally point-scale (i.e., studies are done at a specific location or an experimental station) but at a spatial-scale (e.g., county level) studies are limited. Since a national or a state scale agricultural planning (including agricultural water allocation) cannot be done based on point-scale studies, county-scale studies are critical and their importance is undeniable.

Generally, crop models such as Decision Support System for Agrotechnology Transfer (DSSAT) (Jones et al., 2003) can simulate the IWR using the water balance approach (Tsuji et al., 1998). However, these widely applied models were developed for point-based studies and cannot simulate crop yield or IWR at a gridded-scale. Recently Alderman (2021) developed a parallel gridded simulation framework for DSSAT; however, the input dataset (outputs) are required (generated) in NetCDF format (which is not user-friendly), increasing its difficulty to use. Moreover, the modeling framework requires several soil characteristic datasets at grid-scale (i.e., the infiltration rate and drainage) which are available at very coarse spatial resolution (~20–25 km), limiting its application for county-scale studies. Additionally, since the gridded version of DSSAT simulations is done using Message Passing Interface on high performance computing, it requires high expertise to use the model. In contrast, IWR models such as CROPWAT (Smith, 1992), are simple and can be shared within multiple cores of a single personal computer for parallel simulation. Additionally, CROPWAT calculates the amount of irrigation based on the crop water requirement (evapotranspiration demand from crops and soil), which is primarily dependent on the climatic variables, and simple soil characteristics including maximum rooting depth, field capacity, permanent wilting point, and initial soil moisture (all are specific for soil types) which are readily available at a fine grid-scale and can be aggregated at county-scale.

Therefore, given that the available grid-scale global/national-scale models are spatially coarse, data-intensive, and require high technical expertise, a simpler modeling approach that can simultaneously estimate crop yield under different IWR at county-scale is paramount. In order to address this issue, a novel integrated modeling framework was developed in this study utilizing satellite, and ground-based information to assess the potential increase in crop yields under different levels of irrigation relative to rainfed agriculture. The framework was employed for two major cultivated crops (corn and soybean) under droughts at Mobile River Basin (MRB) in the Deep South US, as a case study where rainfed agricultural practice is dominant. Additionally, the developed framework was employed at county-scale, which is also another novelty of this study relative to the traditional IWR and crop yield estimation studies which are generally point-scale studies. The specific objectives are 1) identification of county-scale agricultural drought at MRB; 2) establishing relationships among drought and rainfed crop yields (corn and soybean); and 3) developing an integrated modeling framework of IWR and crop yield simulation models to assess the potential increase in crop yield under different irrigation application rates during droughts. The findings of this study can be integrated with a robust weekly to seasonal weather prediction system in devising better irrigation water management policies in the region and the novel framework developed is also be applicable at any rainfed agriculture dominant region to combat yield losses encountered during droughts.

2. Study area and datasets

Fig. 1 displays the study area MRB, highlighted within the US. The basin spans over four states including Tennessee, Mississippi, Georgia, and Alabama comprising approximately 115,200 km^2. Roughly two-thirds of the MRB is contained in Alabama. The flow in the basin is generated from the Upper Appalachian Plateau, located in the north, and drains out in the Mobile Bay, in the south. Forest is the predominant land use, comprising approximately 60% of the basin, while agriculture and urban areas comprise of 26% and 3%, respectively. Additionally, water bodies, streams, and reservoirs comprise the rest 11% in the basin (Warner et al., 2005). Corn is generally sown between mid-March and early-May and is harvested between mid-July and early-September (USDA, 1997). Similarly, soybean is sown between mid-May and mid-June and harvested between early-September and early-October (Balkcom et al., 2014). The predominant soil in the basin is sandy loam (20%

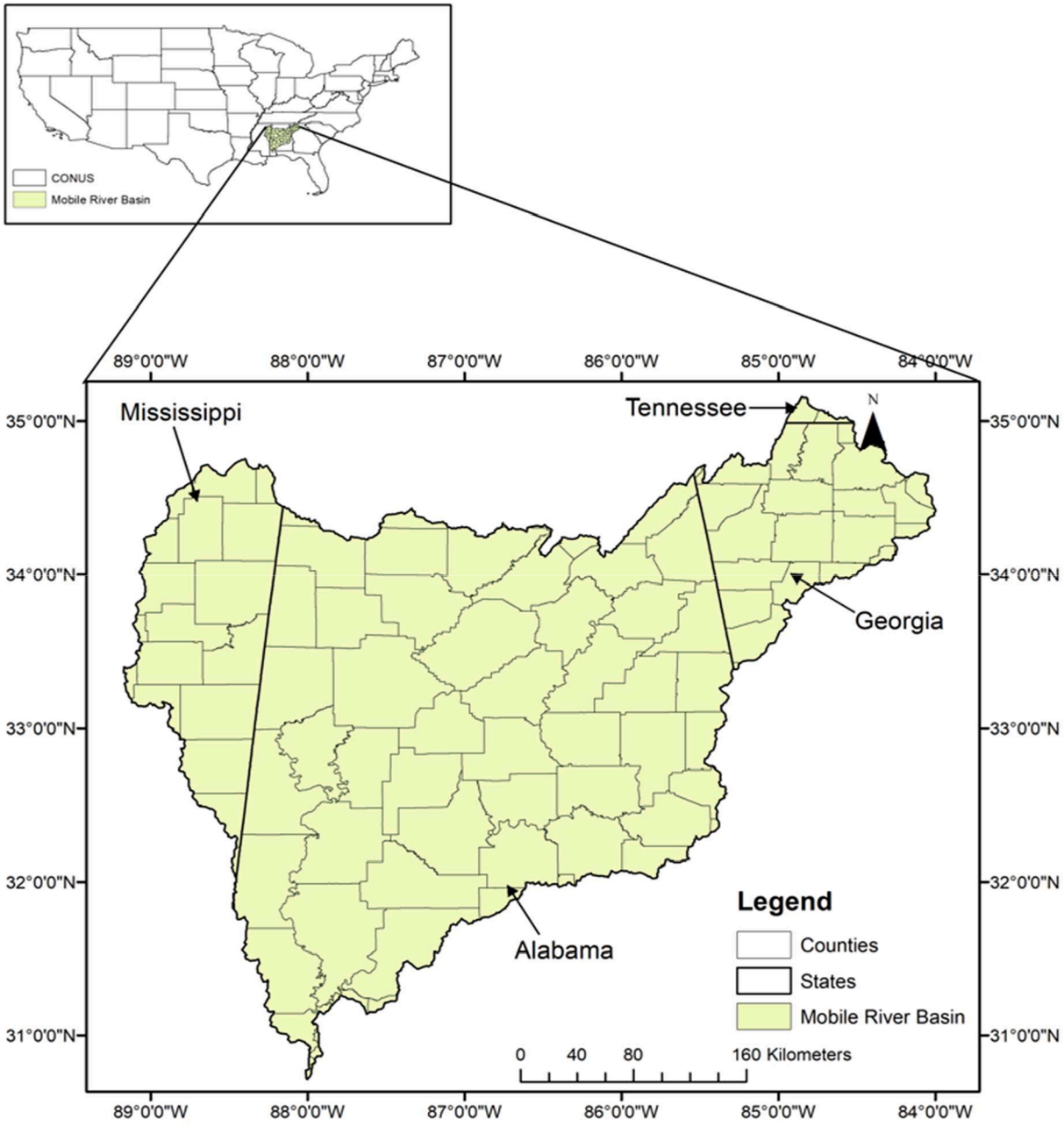

Fig. 1. Location of MRB within the US (top) and the counties and states within the river basin (bottom).

plant available water [PAW]); however, the central region of the basin is characterized by a predominant silty loam soil (15.8% PAW) (Deb et al., 2019; Mitchell et al., 2004). The average annual discharge of the basin at the Mobile Bay is approximately 1760 m3s-1 and ranks as the fourth largest discharge in the US. The basin is comprised by 101 counties which were considered in this analysis (Fig. 1). The average annual precipitation and temperature range from 1270 to 1524 mm and 15 °C (in the north) to 21 °C (in the south), respectively; 65% of the precipitation occurs during the cropping season of corn and soybean. The major agricultural crops comprise corn, soybean, cotton, and hay. Approximately 67% of the cropped area is rainfed, while 27% is irrigated and concentrated in Georgia (~33.6%), Tennessee (3.5%), and Mississippi (~44.4%) states (NRCS, 2017). The most grown corn cultivar/variety in MRB is Pioneer 1319 (Glass et al., 2016); whereas for soybean, Asgrow 46X6 is mostly grown in Alabama, and USDA-N8002 is grown in Georgia, Tennessee, and Mississippi states (Glass et al., 2018).

In order to pursue the study, several datasets were required including meteorological data, soil characteristics, groundwater data, crop-specific information and crop management data, satellite–based actual evapotranspiration (ET_c), and soil moisture data. The details of the datasets used in the study are provided in Table 1.

In addition to the above mentioned datasets, average county-scale crop yield data was collected from the National Agricultural Statistics Service (NASS), United States Department of Agriculture (USDA). This dataset comprises of the average crop yield from irrigated and rainfed cropping conditions. Since rainfed corn and soybean yields play a critical role in this study, particularly in achieving objective two and calibration/validation of the models (discussed later), additional crop yield datasets were also collected from the state agricultural research centers, particularly, Auburn University Alabama Agricultural Experiment Station (Alabama), Mississippi State University Agricultural and Forestry Experiment Station (Mississippi), University of Georgia Cooperative Extension on Crop and Soil Sciences (Georgia), and University of Tennessee Institute of Agriculture (Tennessee). These research centers

Table 1
Datasets, their spatial and temporal resolutions, and their sources used in this study. Note: temporal datasets were collected for the period 2008 – 2019.

Data	Spatial resolution	Temporal resolution	Source
Precipitation	4 km	Daily	PRISM (https://prism.oregonstate.edu/)
Temperature	4 km	Daily	PRISM (https://prism.oregonstate.edu/)
Solar radiation	12.5 km	Daily	NLDAS-2 (https://ldas.gsfc.nasa.gov/nldas/nldas-2-model-data)
Wind speed	12.5 km	Daily	NLDAS-2 (https://ldas.gsfc.nasa.gov/nldas/nldas-2-model-data)
Relative humidity	12.5 km	Daily	NLDAS-2 (https://ldas.gsfc.nasa.gov/nldas/nldas-2-model-data)
Soil hydraulic conductivity	1 km	–	Dai et al. (2019)
Soil texture	1 km	–	Dai et al. (2019)
Groundwater table	–		USGS (https://nwis.waterdata.usgs.gov/usa/nwis/gwlevels)
Cultivar characteristics	–	–	Published state government reports
Crop management	–	–	Published state government reports
MODIS ET_c	500 *m*	8-day	https://modis.gsfc.nasa.gov/data/dataprod/mod16.php
Root zone soil moisture	12.5 km	Daily	NLDAS-2 (https://ldas.gsfc.nasa.gov/nldas/nldas-2-model-data)
Shallow zone soil moisture	1 km	2–3 days	Abbaszadeh et al. (2019), Abbaszadeh et al. (2021)

means not applicable.

publish annual crop yield datasets for both irrigated and rainfed conditions for their several research stations where each research station corresponds to a few counties. A simple arithmetic calculation (Eq. (1)) is done to estimate the rainfed corn and soybean yield under rainfed conditions for the unreported counties.

$$Z = \frac{X + Y}{2} \tag{1}$$

where Z is the average crop yield for a county retrieved from NASS (and is available for all the counties), X and Y are the irrigated and rainfed crop yields, respectively retrieved from the research stations. From Eq. (1) Y (rainfed crop yield) can be calculated for the unreported county as in Eq. (2).

$$Y = (2 \times Z) - X \tag{2}$$

It is to be noted that the irrigated crop yield is assumed to be the same as the crop yield reported in the nearby regional research station as per the suggestion of Novak et al. (2008).

3. Methods

The methods employed in this study can be divided into two phases where Phase 1 addresses the first and second objectives, and Phase 2 addresses the third objective (Fig. 2). Furthermore, Phase 1 can be classified into three stages; (1) 3-month Standardized Precipitation Evapotranspiration Soil Moisture Index (SPESMI) was calculated at a county-scale within the river basin for the cropping season from March to October for each year [2008 – 2019]; (2) the rainfed crop yields were mapped at county-scale, and (3) relationships among SPESMI and detrended crop yields were established at the county-scale level where detrending was done by using simple linear regression model (Quiring and Papakryiakou, 2003). Finally, in Phase 2 potential avoidance of drought-affected rainfed crop yield loss under irrigation was estimated

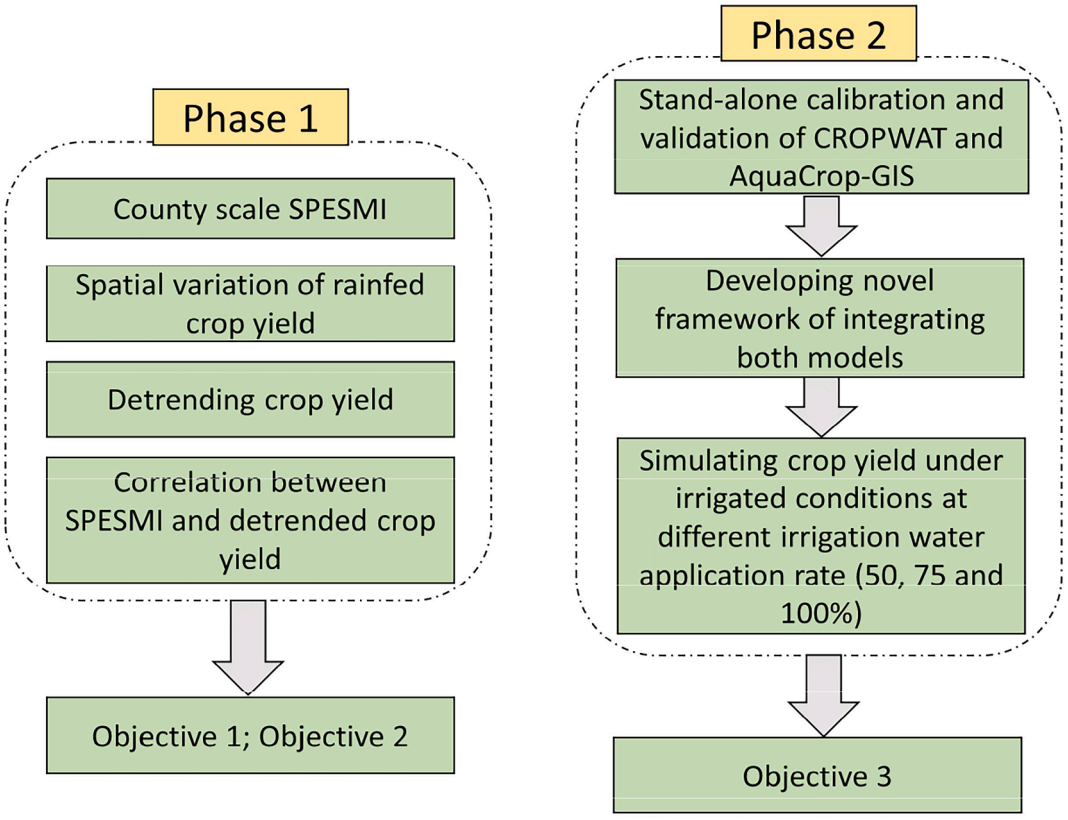

Fig. 2. Flowchart displaying the tasks undertaken in this study to achieve the three objectives.

by employing a novel integrated framework of two models at the county-scale. All of these tasks are provided in detail in the following sections.

3.1. Calculation of Standardized precipitation evapotranspiration soil moisture index (SPESMI)

Identifying agricultural drought years was a crucial step in this study and SPESMI was used to identify those years. SPESMI is a non-parametric multivariate drought index which was developed by combining the marginal probability distributions of root zone soil moisture and the differenced variable of precipitation and evapotranspiration (Xu et al., 2020). Time series of 3-month SPESMI was calculated at a grid-scale of 12.5 km spatial resolution using the 40–100 cm soil moisture information derived from the Noah land-surface model of the North American Land Data Assimilation System (NLDAS-2). The Noah outputs were used due to their superior performance over other model outputs in the Deep Southern states (Xia et al., 2015). In this study, the approach developed by Xu et al. (2020) was used to calculate grid-scale SPESMI. The SPESMI was developed based on the copula function (as suggested by Masud et al., 2015) of the joint probability of root zone soil moisture and the differenced variable of precipitation and evapotranspiration. The main merit of this approach is that it can be employed for two different variables with diverse marginal distributions (Madadgar & Moradkhani, 2013). Since Xu et al. (2020) gave a comprehensive description of the SPESMI, only a brief introduction is presented in this paper. The joint cumulative distribution function (CDF) among precipitation and the differenced variable is expressed in Eq. (3).

$$P(X \le x, Y \le y) = C[F_1(X), F_2(Y)] = C(u_1, u_2) \quad (3)$$

where X and Y are soil moisture and the differenced variable of precipitation and evapotranspiration, respectively, the copula is denoted by C, F_1 and F_2 are the CDFs of X and Y, respectively. Prior to the CDF estimation, X and Y variables were calculated by subtracting the monthly averaged values for each grid for the cropping season. Since ET_c was available at a spatial resolution of 500 m, it was aggregated at 4 km spatial resolution for consistency with the Parameter-elevation Regressions on Independent Slopes Model (PRISM) precipitation dataset. Because PRISM dataset accounts for physiographic features such as variability in terrain, it is considered superior to other datasets (Molter et al., 2021) and hence was used in this study. The Y variable (the difference between precipitation and evapotranspiration) was further regridded to 12.5 km to match the spatial resolution of the root zone soil moisture. All of these conversions were done using ArcPy scripts. The calculated SPESMI outputs representing each grid of 12.5 km spatial resolution were averaged at county-scale using the Zonal Statistics tool in ArcPy programming to represent the county-specific SPESMI values. Additionally, in order to determine agricultural drought year, 3-month SPESMI outputs (March to October; crop growing season) for each county were calculated and then temporally averaged for the duration, representing yearly mean SPESMI from 2008 to 2019. Similar to the drought classification of Standardized Soil Moisture Index (SSMI) and Standardized Precipitation Index (SPI) by McKee et al. (1993), SPESMI was classified into eight categories which are given in Table 2. The agricultural drought year in this study was defined as the year with over 50% of counties experiencing any drought of intensity more than mild dry conditions (Table 2). In this study, normal precipitation year was defined as the years when over 65% of counties comprised of SPESMI values were within the range of −0.49 to 0.50.

Table 2
Drought classification based on SPESMI values.

SPESMI values	Drought class
SPESMI ≥ 2.00	Extreme wet
1.50 ≤ SPESMI ≤ 1.99	Severe wet
1.00 ≤ SPESMI ≤ 1.49	Moderate wet
0.50 ≤ SPESMI ≤ 0.99	Mild wet
−0.49 ≤ SPESMI ≤ 0.49	Normal
−0.99 ≤ SPESMI ≤ -0.50	Mild dry
−1.49 ≤ SPESMI ≤ −1.00	Moderate dry
−1.99 ≤ SPESMI ≤ −1.50	Severe dry
SPESMI ≤ −2.00	Extreme dry

3.2. Spatial and temporal mapping of rainfed crop yields

Before establishing the relationship between drought and crop yields, identifying spatial and temporal variations of the crop yield was essential. Therefore, county-scale annual rainfed corn and soybean yields were extracted from the National Agricultural Statistics Service (NASS), United States Department of Agriculture (USDA), and plotted to represent their spatial and temporal variability. The time period considered to assess this variability was from 2008 to 2019. Several county-specific yield values of the NASS dataset of 2008 and 2009 were missing and hence, the multiple imputation approach (Rubin, 1987) was employed to infill the missing values. In the multiple imputation approach, first the missing values were replaced by random imputed values which were sampled from the predictive distribution of the observed data. These imputations were done to generate multiple datasets. Secondly, standard statistical methods were used to fit a model (regression) to each imputed dataset. Finally, outputs of the multiple models were combined to generate the single imputed value. The multiple imputations were identified to be the most appropriate method in imputing missing crop yield data of NASS and further details on this approach can be found in Lokupitiya et al. (2006).

3.3. Relationship among SPESMI and detrended rainfed crop yield

Generally, crop yields are associated with stochastic trends and climate variability (Schauberger et al., 2018). The stochastic trend component reflects the contribution of several factors including management practices and technological advances, whereas, the climate variability component (includes climate disasters) can induce high-frequency fluctuations such as droughts affecting the crop yield (which is the focus of this study) (Lu et al., 2017). To establish the relationship between the drought index and crop yields, it is crucial to remove the trend component from the yield values. Therefore, based on the finding of Yu et al. (2018), the Hodrick-Prescott (HP) filter was applied on time series of rainfed corn and soybean yield data. The details of the HP filter algorithm can be found in Harvey & Trimbur (2008). In this study, *hpfilter* code within mFilter package in R programming language was run across all the counties to detrend the corn and soybean yields.

Post detrending the yield values, the Pearson correlation coefficient was derived among time series of annual SPESMI values and detrended corn and soybean yields at the county-scale. The correlation coefficient is a measure of the drought impacts on rainfed crop yields.

3.4. Modeling crop yield under irrigation during drought years

Since field experimental trials to assess water requirement are painstaking and time-consuming, in this study, a coupled modeling approach of integrating a deterministic IWR model (CROPWAT 8.0) (FAO, 1992) and a water-driven spatial crop yield simulation model (AquaCrop-GIS) (FAO, 2017; Steduto et al., 2009) was developed to assess the potential increase in crop yields under irrigation relative to rainfed yields during the drought years.

3.4.1. Models' description

To pursue this study the models chosen were CROPWAT 8.0 and AquaCrop-GIS. CROPWAT is one of the robust and widely used IWR estimation models and hence is used in this study. Moreover, the AquaCrop-GIS model was chosen for crop yield estimation since it is a water-driven model and since this study deals with drought (water

stress), it was the best fit. More details on the model are given below.

3.4.1.1. Cropwat 8.0. CROPWAT is a Microsoft Windows based computer program developed by the Food and Agricultural Organization (FAO) for irrigation planning and management. The specific applications of this model include calculating reference evapotranspiration (ET_o), crop-specific actual evapotranspiration, crop water requirement, crop irrigation requirement, and irrigation scheduling. The model calculates reference evapotranspiration by employing the Penman-Monteith equation (Allen et al., 1998). Then, ET_o is further used to calculate the ET_c in Eq. (4).

$$ET_c = Kc \times ET_o \tag{4}$$

where ET_c is actual crop evapotranspiration (mm day^{-1}), ET_o is reference evapotranspiration (mm day^{-1}) and *Kc* is crop coefficient. Daily root zone soil water balance is employed in the computation of the IWR and the outputs are calculated at 10-days intervals. Additionally, the irrigation schedule accounting for the amount and irrigation timing is also stored separately for the cropping season. The model requires daily climate data (precipitation, temperature, relative humidity, sunshine duration, and wind speed), soil data (maximum rooting depth, field capacity, permanent wilting point, and initial soil moisture), and crop information (crop type, planting, and harvesting dates, and days of each crop stage). The model also requires four parameters to be calibrated for optimal model performance. These parameters are primarily the crop coefficients (k_c) (Eq. (4)) during different crop growth stages, which are initial (Kc_{ini}), development (Kc_{dev}), middle (Kc_{mid}), and late (Kc_{lat}). The model also allows users to couple with an external model parameterization software or algorithm for model optimization. Although the model has several outputs (as mentioned above), the main outputs used in this study were the IWR and irrigation scheduling. Further details on the model can be found in FAO (1992).

3.4.1.2. AquaCrop-GIS. AquaCrop-GIS is a spatial-scale (user-defined spatial information required, either grid-scale or administrative level) crop yield simulation model that uses the widely used water-driven AquaCrop model in its core. The model is a Microsoft Windows based program to simulate the crop yield at a user-defined spatial-scale. Seven classes of datasets are required for yield simulation. These datasets include crop information, details of the soil initial condition, soil type data, groundwater table data, management details (including planting, weeding, irrigation, and harvesting dates), weather data (precipitation, temperature, and ET_o), and study area map (.shp format file).

The versatility, applicability (Deb et al., 2015; Shrestha et al., 2014), and the lesser input data requirement (Babel et al., 2019) of the AquaCrop model is the primary reason for its selection in this study. The model uses normalized water productivity and the ratio of transpiration to ET_o to calculate above-ground biomass (Eq. (5)). Also, the yield is considered and calculated as a function of reference harvest index and above-ground biomass (Eq. (6)).

$$B = Ks_b \times WP^* \times \sum \frac{T_r}{ET_o} \tag{5}$$

$$Y = f_{HI} \times HI_o \times B \tag{6}$$

where B is above-ground biomass (kg m^{-2}), Ks_b is air temperature stress coefficient, WP* is normalized water productivity (kg m^{-2} mm^{-1}), T_r is transpiration (mm day^{-1}), ET_o is reference evapotranspiration (mm day^{-1}). Y is crop yield (kg m^{-2}), f_{HI} is the adjustment factor for all stresses affecting crop yield, HI_o is the reference harvest index and B is above-ground biomass. Further details on the model can be found in Steduto et al. (2009).

3.4.2. Integrating irrigation water requirement (IWR) and crop yield simulation models

The spatial estimation of crop yield under irrigation can be assessed by three approaches: (1) using a crop yield simulation model (with IWR as input either calculated or simulated by another model); (2) integration of IWR model and crop yield simulation model; and (3) developing a new model/code while considering both components (i.e., calculation of IWR and crop yield simulation). While the first option is the simplest, it is not feasible since the exact amount of IWR under droughts is unknown and manual calculation at a grid- or county-scale is simply impractical. Similarly, the third option has its own disadvantages including data constraints and computational limitations associated with its testing and validation prior to its application. On the other hand, the second option provides the flexibility of choosing different models and is more robust since the chosen models are well developed and applied in diverse regions around the world. Therefore, in this study, the second option was selected using CROPWAT 8.0 and AquaCrop-GIS models, previously described. Although the traditional AquaCrop model can simulate IWR, the "percentage of readily available water in the root zone" data is not readily available at county-scale and requires intensive field/laboratory testing. Moreover, scaling up this variable from field/laboratory to county/grid-scale is impractical. On the other hand, CROPWAT uses simple soil characteristics, particularly total available soil moisture (which is constant for a particular soil type and fine resolution soil maps are available), and climatic variables such as maximum, minimum temperature, relative humidity, precipitation, solar radiation, and wind speed to simulate IWR and irrigation scheduling and therefore used in this study. More importantly, the integrated modeling framework is easy to implement and does not require much technical expertise or intense coding.

In the integrated modeling framework, both the CROPWAT and AquaCROP-GIS models are loosely coupled to diminish the model component interdependencies and increase the flexibility of the framework as it allows users to altercate the models. Basically, it consists of three major steps: (1) stand-alone calibration and validation of CROPWAT and AquaCrop-GIS for normal precipitation years; (2) simulation of IWR and irrigation scheduling by CROPWAT under drought conditions; (3) using the IWRs from CROPWAT as input in AquaCrop-GIS to simulate the crop yield during drought years. Given that AquaCrop-GIS is a spatial model, the model setup within the study domain is relatively simple (in terms of model setup) compared to the CROPWAT model, where the latter is required to be set for each county (in this study).

3.4.2.1. Model calibration and validation. Both models were calibrated independently using a the Shuffled Complex Evolution (SCE) algorithm (Duan et al., 1994; Duan et al., 1993), a widely used stochastic global optimization algorithm. In this approach, first stochastically a sample of points is distributed over the parameter space within the lower and upper bounds. Every sample point is considered as a member of the population and each individual is characterized by its unique genetic information. By altering the genetic information i.e., the parameter values, the population tends to direct towards an optimum, which is the optimum of the objective function corresponding to the model simulated values and the observed values. The initial sample of the population is also divided into several sub-samples (also called complexes). Each combination of complexes produces offspring following the simplex procedure of Nelder & Mead (1965). The likelihood of an individual in reproduction depends on its fitness. The older points are then replaced by the offspring. This proceeds towards a global optimum which is assisted by (a) a probability that new points are spontaneously created within the feasible parameter space and (b) a regular combination of the points into new complexes. Further details on the SCE algorithm can be found in Duan et al. (1993).

Since this is a county-scale study and the AquaCrop-GIS model consists of over 40 conservative and non-conservative model

parameters, sensitivity analysis is essential to avoid the computational burden. First, the most crucial parameters (12 in total) were identified from the literature (Deb et al., 2015; Shrestha et al., 2016), followed by a sensitivity analysis (Table 3). Each parameter was adjusted by ± 15% (Deb and Kiem (2020); Uniyal et al. (2019)) relative to their default value and a model simulation was done for the year 2015 keeping other parameters to their default values. Based on the |percentage change in yield|, the parameters were classified as "high" (>% 10), "moderate" (5%-10%), and "low" (<5%) sensitive parameters based on the range of the absolute value of percent change in the simulated yields corresponding to the changed parameter value relative to the default parameter value. The criteria used in this study was set by Geerts et al. (2009). In this study only the high and moderate sensitive parameters were selected for the model calibration. It is to be noted for reducing computation burden, the sensitivity analysis was done for only one corn and soybean growing county within the Alabama state (Dallas) where both the crops were grown intensively. Also, the sensitivity analysis was done for the Pioneer 1319 cultivar of corn (grown in the entire MRB) and the Asgrow 46X6 cultivar of soybean (grown in Alabama). The USDA-N8002 cultivar of soybean (which is mostly grown in Tennessee, Mississippi, and Georgia states) was not used in the sensitivity analysis due to similarity in physiological characteristics with the Asgrow 46X6 cultivar.

The CROPWAT model consists of four coefficients (crop coefficients based on the crop growth stages, which are initial, development, middle, and late) which were optimized by linking the model with the SCE algorithm. The AquaCrop-GIS model was calibrated against the annual corn and soybean yield for normal precipitation years (2009, 2010, 2013, 2014, 2015, and 2019) and the time series of soil moisture (at daily time-step) for the year 2015 (since a majority of the counties received precipitation around the 30-year average rainfall) against 1-km downscaled soil moisture (5 cm) for Conterminous United States (CONUS) developed by Abbaszadeh et al. (2019). Since AquaCrop-GIS simulates the soil moisture on a volumetric basis (i.e., m^3/m^3), the moisture content for the top soil layer (5 cm) simulated by AquaCrop-GIS is calculated by multiplying 50 to the volumetric soil moisture simulated by AquaCrop-GIS. This results in soil moisture in mm water per 5 cm depth of soil per unit area, which is compared against the 1-km downscaled soil moisture. CROPWAT model was calibrated against the time series Moderate Resolution Imaging Spectroradiometer (MODIS) 500 m resolution ET_c data (MOD16A2) available at the 8-day interval for the year 2013 since the year was a normal precipitation year. Both models were calibrated at county-scale and the spatially varying calibration parameters were stored with county IDs in two data frames (one for CROPWAT and another for AquaCrop-GIS) for use in simulation. Post calibration, both models were also validated at the study basin. Since the time series of crop yield data was limited, AquaCrop-GIS model was validated against time series of volumetric soil moisture content (derived from Abbaszadeh et al. 2019) for the year 2018 (normal precipitation year and not to overlap the year for CROPWAT calibration) at county-scale. Similarly, for CROPWAT validation at county-scale, the model simulated time series ET_c was compared against 8-day MODIS ET_c for the same year (2018). For evaluation of the model performance, Nash-Sutcliffe Efficiency (NSE), coefficient of determination (R^2), and correlation coefficient were used. Further details on these evaluation metrics can be found in Moriasi et al. (2007).

Table 3
The 12 AquaCrop-GIS model parameters with their upper and lower bounds used in the sensitivity analysis and their default values.

Parameters	Description	Lower bound	Upper bound	Default value
MCC	Maximum Canopy Cover (fraction)	0.56	1.0	0.63
CGC	Canopy growth coefficient (% day^{-1})	5.0	22.0	13.0
CDC	Canopy decline coefficient (% day^{-1})	2.0	10.0	5.5
RTX	Maximum effective rooting depth (m)	0.84	1.56	1.10
P_{upper}	Water stress coefficient for canopy expansion (upper) (fraction of Total Available Water (TAW))	0.455	0.845	0.635
P_{lower}	Water stress coefficient for canopy expansion (lower) (fraction of TAW)	0.14	0.26	0.17
PSENSHP	Water stress coefficient curve shape (−)	2.1	3.9	2.85
SSC	Stomatal stress coefficient	1.75	3.25	2.60
ASC	Aeration stress coefficient	0	1.0	0.43
HI_{LF}	Coefficient, Harvest Index (HI) increased by inhibition of leaf growth at anthesis	0	3	0.70
HI_{LBF}	Coefficient, HI reduced by inhibition of leaf growth at anthesis	0	1	0.20
Ks_{sen}	Canopy senescence stress coefficient	0	1	0.40

3.4.2.2. Simulating irrigation water requirement (IWR) and irrigation scheduling for drought years. Once the CROPWAT model was calibrated at each county for the year 2013, the model was used in simulating the IWR and irrigation scheduling for the drought years derived from the step described in Section 3.1 over the entire basin. The time-variant input variables (i.e., precipitation, temperature, relative humidity, sunshine duration, and wind speed) were used only for the cropping duration i.e., from March to October for each year in the simulation.

3.4.2.3. Integrating CROPWAT and AquaCrop-GIS. A schematic representation of the integration of both models is shown in Fig. 3.

As mentioned earlier both models were loosely coupled in the integrated simulation phase where the outputs of the CROPWAT model were forced in the AquaCrop-GIS model. Post calibration of the CROPWAT model, the input variables (climate, soil, and crop data) were forced into the model for simulating the IWR of the crops for the drought years. The model simulates IWR at 10-day intervals and the county-scale 10-day period IWR was calculated. Additionally, the model also simulates irrigation scheduling where the amount of irrigation water and the timing of irrigation are calculated. Based on the irrigation amount calculated in this step, the irrigation water application rates were calculated for 50%, 75%, and 100% (full) of the net irrigation requirement. These irrigation water application rates were calculated for each county and values were stored into time series of ASCII files for the cropping season corresponding to the irrigation timing. It is worth mentioning that the cumulative irrigation water amount simulated from the irrigation scheduling step throughout the cropping season gives the total IWR.

In the following step the calibrated AquaCrop-GIS model was forced with calibrated parameters (stored in the data frame) along with the input weather variables, soil, crop, groundwater, initial soil water, crop management data, the county shapefile, and the time series of ASCII files with irrigation information. The final outputs from the model were county scale corn and soybean yield under 50%, 75%, and 100% IWR for the drought years. The simulated yields were then compared against the actual county-scale rainfed yield calculated based on USDA NASS and regional agricultural research stations. The findings are presented in spatial maps for ease of representation.

4. Results

4.1. Identification of drought years

Fig. 4 represents the spatial and temporal variation of the SPESMI representing the agricultural drought in the MRB. The results indicate

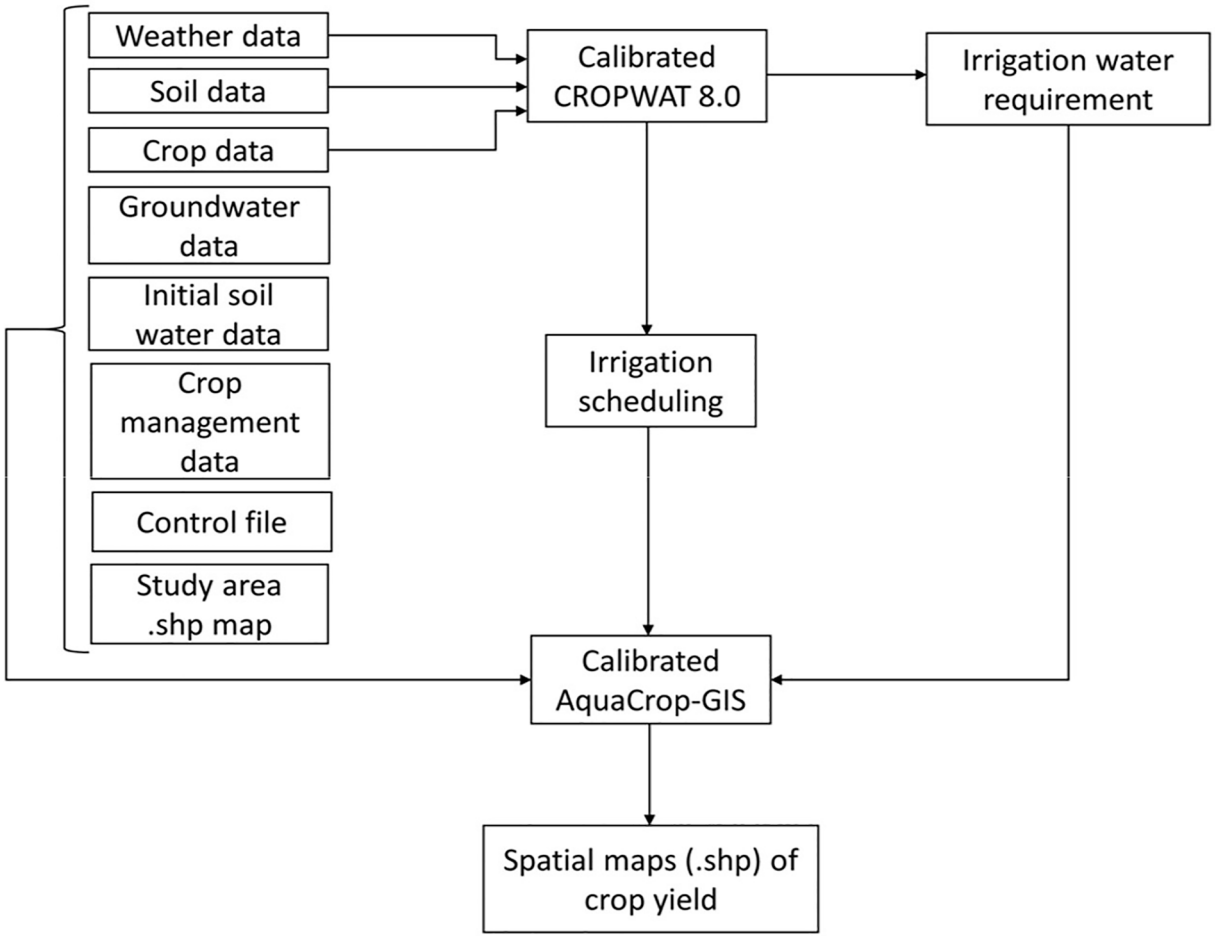

Fig. 3. Flowchart showing the integrated CROPWAT-AquaCrop-GIS modeling framework used to simulate crop yield under irrigation conditions in drought years at MRB.

that a significant part of the MRB experienced droughts in the years 2008, 2011, 2012, and 2016. The drought intensity ranged from mild (SPESMI – −0.50) to severe (SPESMI – −1.99) during the years 2008 and 2011, with severe droughts in the eastern and southern counties for the respective years. Similarly, for 2012 the drought is noted to range from mild to extreme (SPESMI < -2.00) with the eastern counties (east Alabama and Georgia) experiencing severe and extreme droughts. The year 2016 is relatively milder with central Alabama to western Georgia experiencing mild to moderate (SPESMI – −1.49 to −1.00) droughts. These results are consistent with the findings of Xu et al. (2020), where droughts within the range of mild to moderate are noted for the states of Alabama, Georgia, Mississippi, and Tennessee during 2016. Few counties are also noted to experience mild droughts in the years 2009, 2015, 2017, and 2018 (Fig. 4), however, given that the area under drought is <20% of MRB and of mild drought intensity, these years are not considered as the drought years in the preceding analysis.

4.2. Rainfed corn yield

Fig. 5 displays the spatial and temporal variability of rainfed corn yield within MRB. The rainfed corn yield is noted to range from 3.0 t/ha to 12.9 t/ha both spatially and temporally. The lowest corn yields are noted for the drought-affected counties in the years 2008, 2011, 2012, and 2016. Overall in MRB, the year 2012 is observed to have the lowest corn yield (within the range of 3.0 to 6.9 t/ha), with the minimum values in the eastern counties (in Georgia state). Similarly, in the year 2011, the lowest yield is also noted within the same range of 2012, but for the southern counties. For the year 2016, the entire state of Alabama (except for a few counties in the western region) and all Georgia are noted to have an average yield ranging from 4.0 to 6.9 t/ha. During non-drought years, interestingly a lower yield is also noted for the state of Alabama relative to Mississippi (western region) and Georgia. For example, in the case of 2013 (normal precipitation year), Georgia and Mississippi are noted to have an average yield ranging from 8.0 to 8.9 t/ha and 7.0 – 8.9 t/ha respectively, whereas, Alabama consists of an average yield ranging from 6.0 to 6.9 t/ha (except 4 counties in the east). Similar lower yields in Alabama can also be observed for the years 2010, 2015, 2018, and 2019. This poor yield can be attributed to the poor crop management strategies (such as weeding, fertigation, pesticide application, etc.) including hand weeding is practiced within the state of Alabama (Molnar et al., 2011; Duzy et al., 2016). Nevertheless, drought-affected counties over the whole MRB experience reduced rainfed corn yield within the study period.

4.3. Rainfed soybean yield

The areal average rainfed soybean yield for each county throughout the MRB ranges from 0.6 t/ha to 4.0 t/ha during 2008 to 2019 (Fig. 6). The eastern counties of the basin (lying in the state of Georgia and few counties of Alabama) are noted to have an average yield ranging from 1.1 to 1.5 t/ha for the year 2008. The eastern Alabama region is also noted to have an average yield of 1.6 – 2.0 t/ha for the corresponding year. The lowest yields are observed for the counties in southern Alabama and eastern Georgia for the years 2011 and 2012 respectively, with an absolute value of 0.6 to 1.0 t/ha. In contrast to the counties with lowest corn yields concentrated in the central and eastern region of the

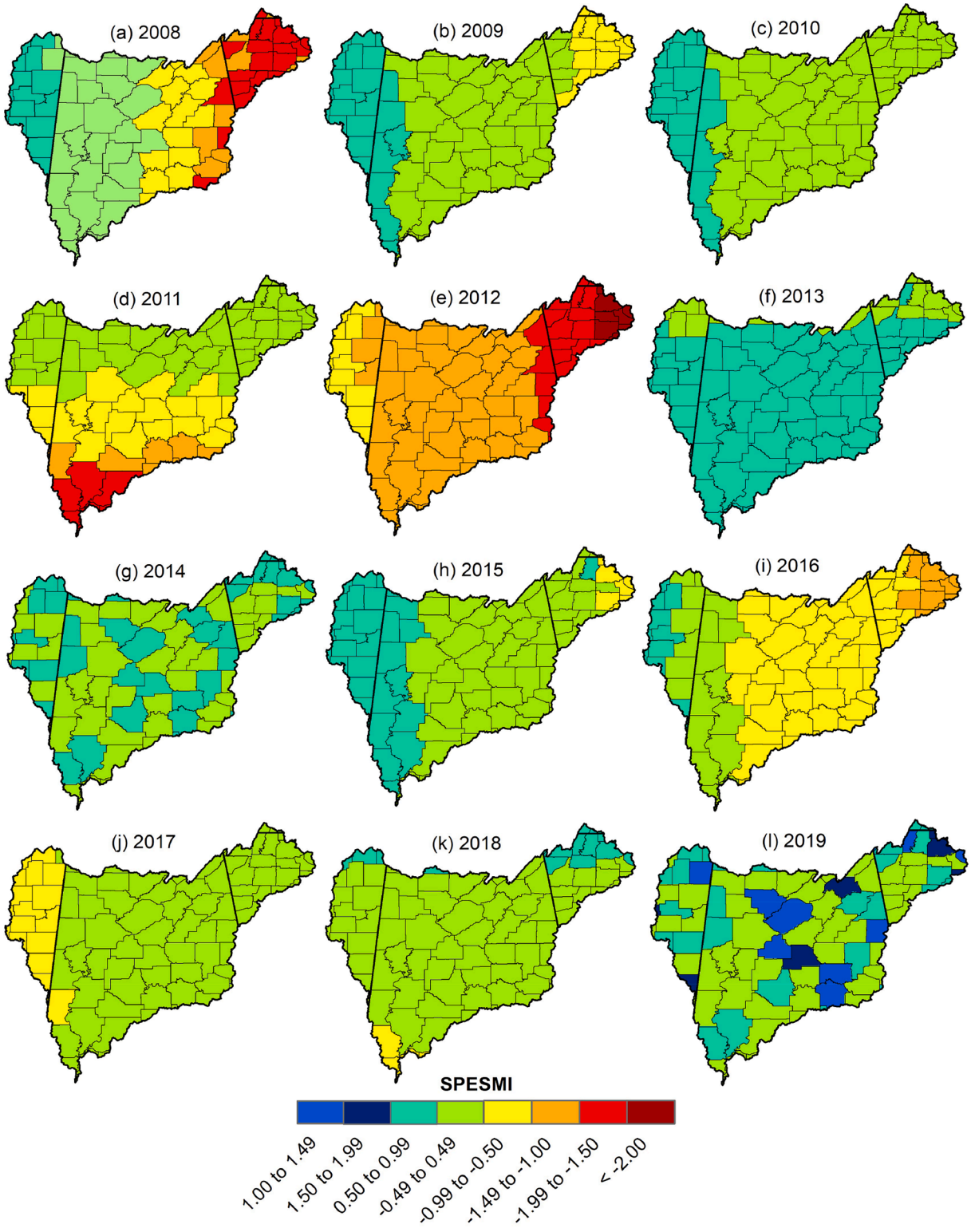

Fig. 4. Spatial and temporal variability of SPESMI (agricultural drought indicator) in the MRB. Drought classification corresponding to the range of SPESMI is based on Carrão et al. (2016).

basin in 2016, the counties with lowest soybean yield (0.6 – 1.0 t/ha) for the same year are distributed throughout the central and eastern region of the basin. It is worth mentioning that all of the counties with yields ranging from 0.6 to 1.5 t/ha have experienced mild to extreme droughts over the study period (2008 – 2019). Similar to the rainfed corn yield, poor soybean yield is also observed for non-drought years in Alabama, for example in the years 2010, 2013, 2018, and 2019, the average soybean yield in Alabama ranges from 2.1 to 3.0 t/ha, whereas, for Mississippi and Georgia, the yield ranges from 3.1 to 4.0 t/ha.

4.4. Relationship between drought and rainfed crop yields

Fig. 7 represents the county-scale Pearson correlation coefficient among the agricultural drought index (SPESMI) and the detrended

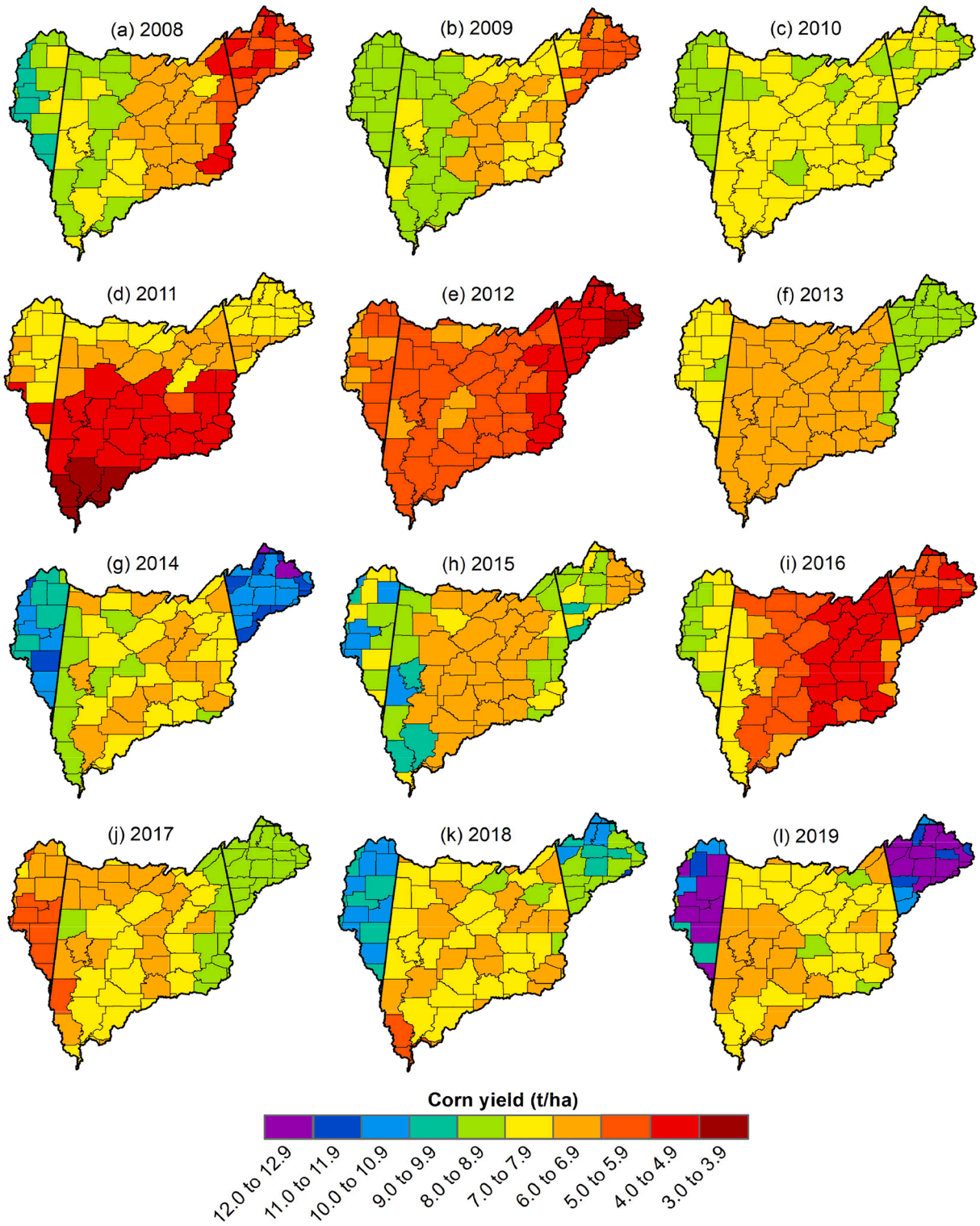

Fig. 5. Spatial and temporal variability of county-scale rainfed corn yield within MRB. Note: years 2008, 2011, 2012 and 2016 are drought years.

rainfed crop yields (corn and soybean) from 2008 to 2019. The results indicate an overall positive correlation among the variables with correlation coefficients ranging from 0.30 to 0.69 for corn and 0.30 to 0.79 for soybean. This indicates that a higher intensity of drought (greater magnitude of SPESMI negative value) results in lower yield across the MRB for both crops. It is important to note that majority of the counties are observed to have a poor to moderate Pearson correlation coefficient (ranging from 0.30 to 0.59) among drought intensity (higher negative value of SPESMI) and detrended rainfed corn yield. This indicates that although a higher magnitude of the drought index hinders the crop yield, yet the effect is not as intense as compared to the soybean yield (where the correlation coefficient is much higher). This potential weak correlation among the detrended corn yield and drought intensity can be attributed to the fact that corn is a C4 plant and has the ability to adapt under elevated carbon dioxide and hot, dry environments to a certain extent (Lara and Andreo, 2011). This is because C4 plants alter the C3

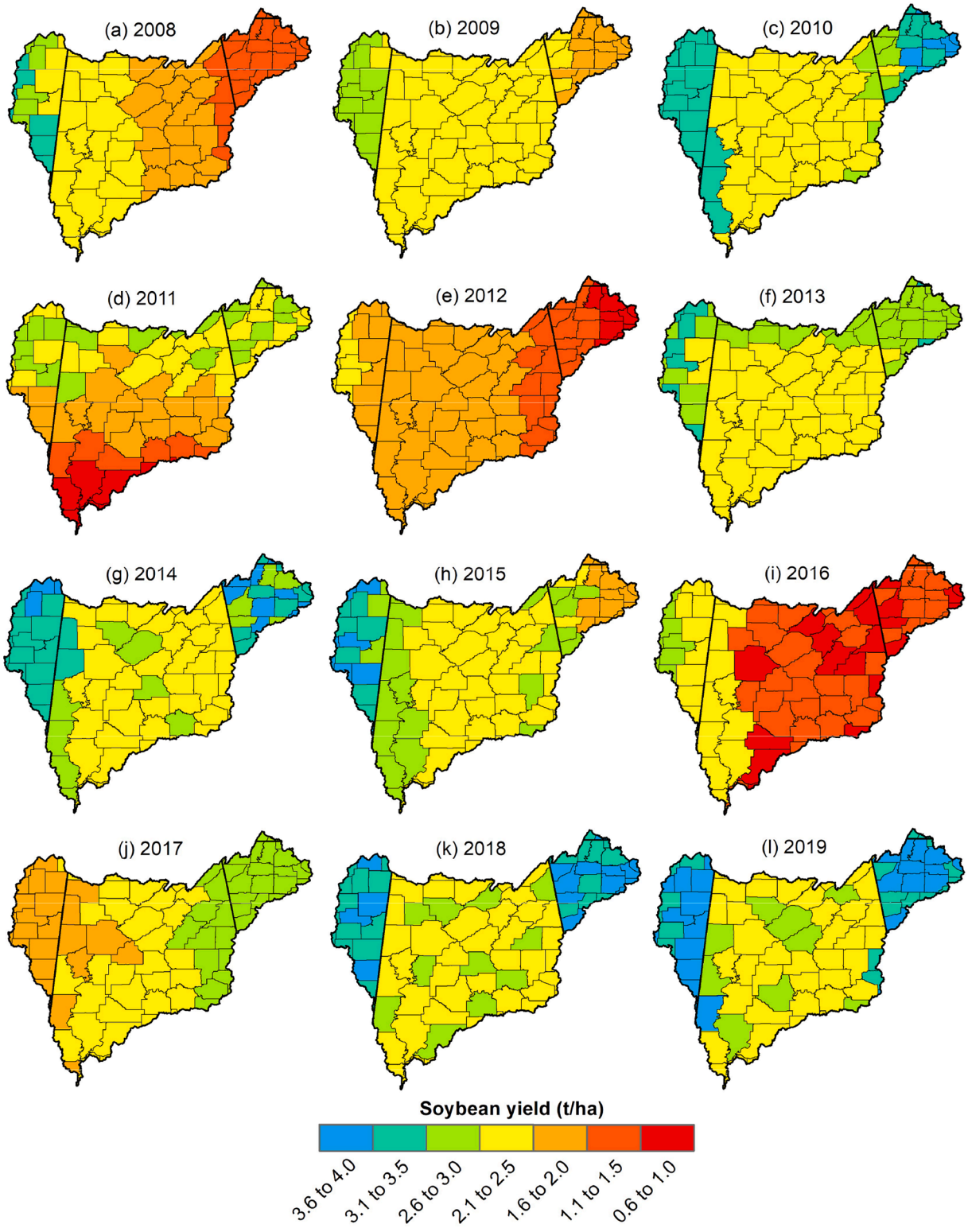

Fig. 6. Spatial and temporal variability of county-scale rainfed soybean yield within MRB. Note: years 2008, 2011, 2012, and 2016 are drought years.

photosynthesis pathway (as in soybean) by minimizing the water loss, reducing photorespiration and increasing the photosynthetic efficiency (Edwards and Walker, 1983). Therefore, yield loss is likely to be reduced under mild and moderate droughts relative to soybean and leads to a poor correlation. Interestingly, the relationship between drought intensity and detrended rainfed soybean yield reveals the highest Pearson correlation values for Alabama state (Fig. 7(b)) with correlation coefficients between 0.5 and 0.8 (majority values ranging from 0.6 to 0.8). This implies that the rainfed soybean yields are more impacted by severe droughts in Alabama relative to other states and corn.

4.5. Standalone model calibration and validation

This section provides the results of the standalone model calibration

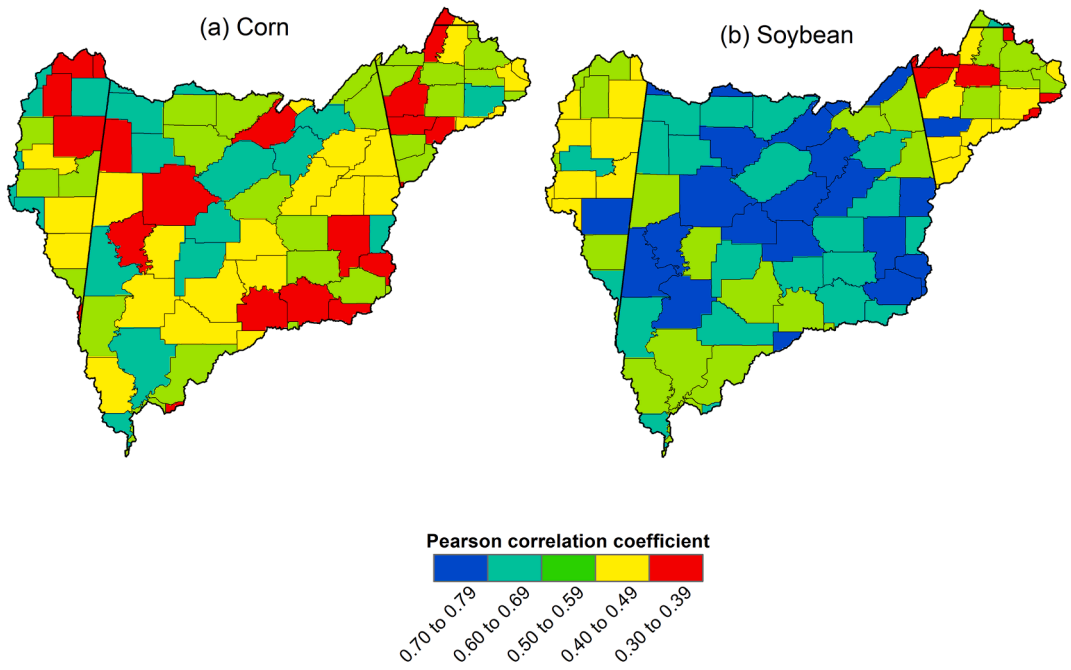

Fig. 7. Spatial variability of Pearson correlation coefficient between SPESMI and detrended (a) corn and (b) soybean yields at county-scale within MRB. Note: Pearson correlation coefficient is calculated based on SPESMI values and detrended annual yields for each county within the basin for the study period of 2008 – 2019.

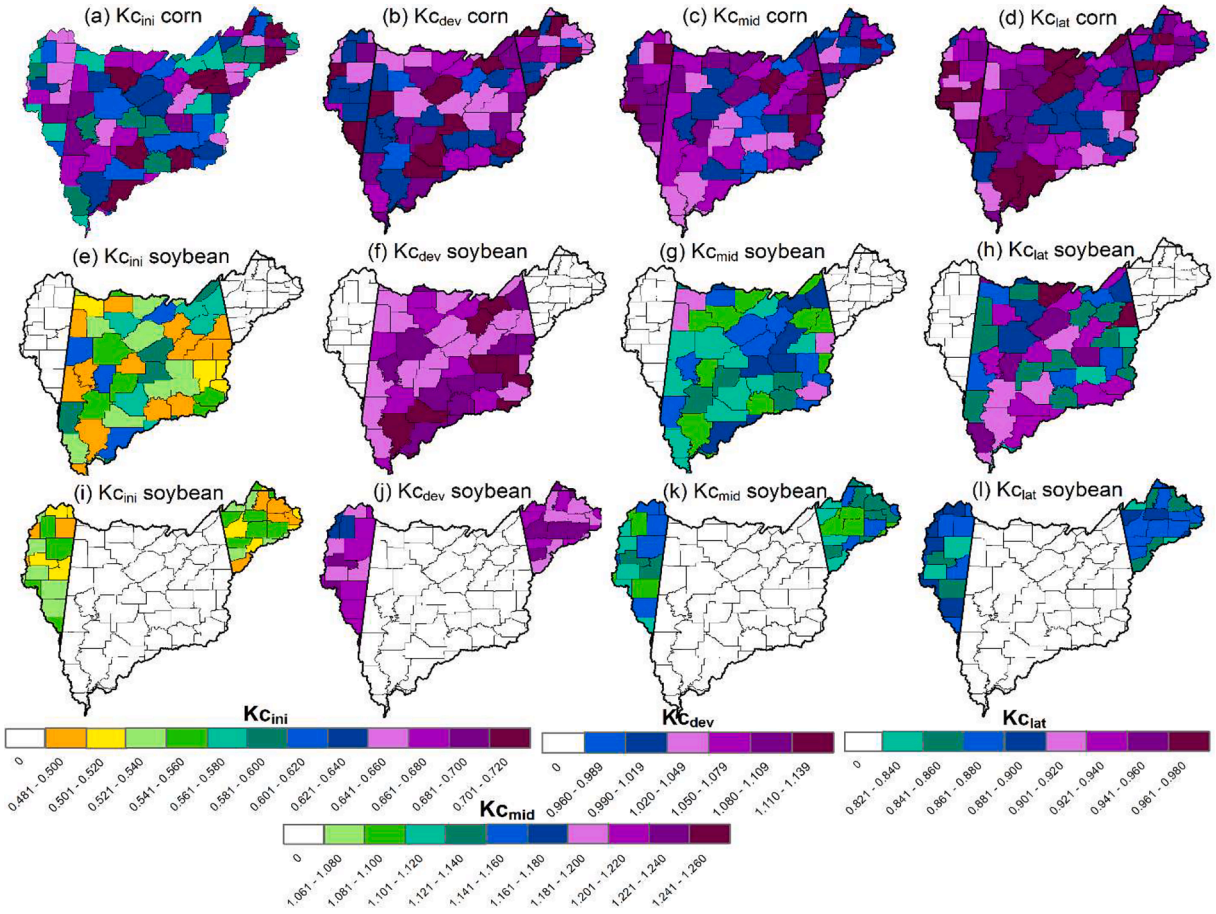

Fig. 8. Spatial variability of stagewise crop coefficients for the CROPWAT model estimated by the SCE algorithm. The adjusted crop coefficients for Kc_{ini} (initial stage), Kc_{dev} (development stage), Kc_{mid} (middle stage), and Kc_{lat} (late stage) are presented in (a), (b), (c), and (d), respectively for Pioneer 1319 cultivar of corn. Similarly, the corresponding four stages for Asgrow 46X6 (grown in Alabama) and USDA-N8002 (cultivated in Georgia, Mississippi, and Tennesse states) are presented in (e), (f), (g), and (h), and (i), (j), (k), and (l), respectively. Note: white color indicates no values in plots (e) to (l).

and validation including the calibration parameters for both CROPWAT and AquaCrop-GIS models.

4.5.1. Cropwat

Fig. 8 represents the stagewise CROPWAT model crop coefficients estimated by the SCE algorithm over the MRB. The initial stage crop coefficient varies widely across the MRB ranging from 0.561 to 0.720 for corn (Pioneer 1319 cultivar), whereas it varies from 0.481 to 0.640, and 0.481 to 0.560 in the case of Asgrow 46X6 and USDA-N8002 cultivars of soybean respectively. In contrast, a lower variation in the crop coefficient is observed for the development stage, where it varies from 0.960 to 1.139 for corn, and 1.020 to 1.139 for Asgrow 46X6 cultivar of soybean, and 0.990 to 1.109 for USDA-N8002 cultivar of soybean. In the case of middle stage of corn, the crop coefficient is observed to vary from 1.141 to 1.260 for corn, and 1.081 to 1.200 (1.061 to 1.160) for Asgrow 46X6 (USDA-N8002) cultivar of soybean. Similarly, for the late stage, the crop coefficient varies from 0.881 to 0.980, and 0.821 to 0.960 (0.821 to 0.900) for soybean cultivar of Asgrow 46X6 (USDA-N8002). Overall, higher values of crop coefficient are noted for corn, followed by the Asgrow 46X6 cultivar of soybean, and the lowest for the USDA-N8002 soybean cultivar.

Based on the optimized values of the crop coefficients during model calibration, Nash Sutcliffe Efficiency (NSE) of 0.56 to 0.90 (with a median value ranging from 0.61 to 0.65) is observed for simulated and MODIS derived ET_c across the MRB in the case of corn (Fig. S2(a)). For the same output variable (ET_c), a relatively higher value of median NSE is noted for Asgrow 46X6 and USDA-N8002 cultivars of soybean ranging from 0.71 to 0.75, and 0.66 to 0.70 respectively (Fig. S2(b)). Overall, throughout the MRB for both soybean cultivars, NSE ranges from 0.61 to 0.85. The difference in the simulated cumulative ET_c and MODIS derived ET_c for corn ranges from −29 to 40 mm for the entire cropping season (from May to October) of 2013. Similarly, for Asgrow 46X6 and USDA-N8002 cultivars of soybean, the difference ranges from −49 to 40 mm for the whole cropping season. Overall, both NSE and difference in ET_c reflect a very good calibrated CROPWAT model throughout the entire MRB.

The CROPWAT model validation reflects NSE ranging from 0.65 to 0.84 for corn across all counties with higher NSE values ranging from 0.69 to 0.84 in the central and the western counties for the cropping season of 2018. The eastern counties display poor model performance with majority of the counties inheriting NSE in the range of 0.65 to 0.72 (Fig. S3(a)). A relatively slight poor performance is observed for the model validation results for soybean across the study area. The NSE for soybean ranges from 0.60 to 0.80 with lower NSE values concentrated in the central and southern region of the basin (Fig. S3(b)). The difference between 8-day accumulated CROPWAT simulated ET_c and 8-day MODIS ET_c also shows an analogous pattern with close to zero values in the central and western counties for corn (Fig. S3(c)). In case of soybean, the difference between MODIS and model simulated ET_c shows values ranging from −39 mm to −20 mm in most of the counties in the western

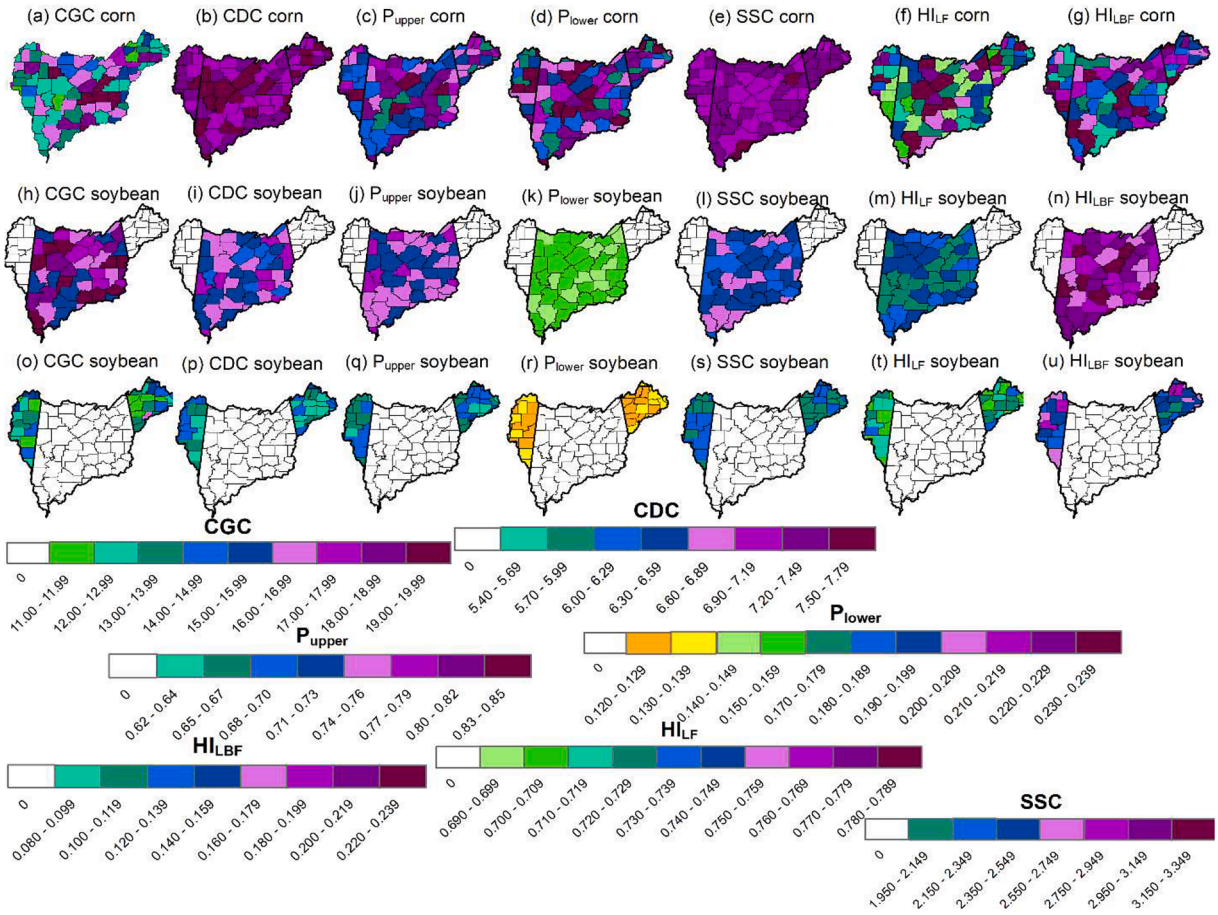

Fig. 9. Spatial variability of calibrated AquaCrop-GIS model parameters using the SCE algorithm. The calibrated model parameters for corn (cultivar Pioneer 1319) are shown in panels (a) to (g), and for Asgrow 46X6 and USDA-N8002 cultivars of soybean are presented in panels (h) to (n), and (o) to (u) respectively. Note: white color indicates no values in panels (h) to (u). Here CGC, CDC, Pupper, Plower, HILBF, HILF, and SSC represent canopy growth coefficient (% day-1), canopy decline coefficient (% day-1), water stress coefficient for canopy expansion (upper) (fraction of Total Available Water (TAW)), water stress coefficient for canopy expansion (lower) (fraction of TAW), coefficient of HI reduced by inhibition of leaf growth at anthesis (-), coefficient of Harvest Index (HI) increased by inhibition of leaf growth at anthesis (-), and stomatal stress coefficient (-), respectively.

and central region, whereas, higher positive values in the range of 21 mm to 40 mm in the eastern counties (Fig. S3(d)). These results indicates the model performs slightly better for corn relative to soybean in the study area, although the magnitude of both NSE and difference in ET_c estimates indicates CROPWAT model performance is acceptable for both crops.

4.5.2. AquaCrop-GIS

Fig. 9 represents the spatial variability of the calibrated AquaCrop-GIS model parameters across MRB. As identified in the sensitivity analysis seven model parameters are considered in the optimization (Tables S1 and S2). The parameters canopy growth coefficient (CGC; ranges between 5.0 and 22.0), coefficient, harvest index increased by inhibition of leaf growth at anthesis (HI_{LF}; ranges between 0.0 and 3.0), and coefficient, harvest index reduced by inhibition of leaf growth at anthesis (HI_{LBF}; ranges between 0 and 1.0) vary widely across the river basin for corn ranging from 11.00 to 19.99 (Fig. 9(a)), 0.690 to 0.789 (Fig. 9(f)), and 0.080 to 0.239 (Fig. 9(g)) respectively. On the contrary, for soybean cultivars the variability of the corresponding model parameters are slender (Fig. 9(h), (m), (n), (o), (t), and (u)). Interestingly, it can also be seen that the calibrated values of all model parameters are lower for soybean crop relative to corn. Moreover, the calibrated values are noted to be lower for the USDA-N8002 cultivar compared to the Asgrow 46X6 cultivar.

The spatial variation in the AquaCrop-GIS model performance during model calibration is shown in Fig. S4. The coefficient of determination (R^2) of corn and soybean yields ranges from 0.70 to 0.87, and 0.79 to 0.93 respectively (Fig. S4(a and b)). Similarly, the R^2 among the AquaCrop-GIS simulated shallow soil moisture (5 cm) and 1-km soil moisture derived from Abbaszadeh et al. (2019) indicates variability from 0.70 to 0.87 and 0.73 to 0.90 for corn and soybean cropping seasons respectively. Since $R^2 \geq 0.70$ throughout the MRB, using the criteria set by (Moriasi et al., 2007), the model is well calibrated.

For AquaCrop-GIS model validation the correlation coefficient among model simulated and observed soil moisture is noted to range from 0.56 to 0.90 for corn and 0.56 to 0.85 for soybean across the MRB (Fig. S5(a and b)). Similarly, the R^2 ranges from 0.66 to 0.90 and 0.60 to 0.85 for the corresponding crops (Fig. S5(c and d)). Similar to CROPWAT model, a slightly better performance in model simulations is observed for corn crop compared to soybean at the study area. A lower correlation coefficient and R^2 is observed in the central region for soybean. Nevertheless, both correlation coefficient and R^2 suggests AquaCrop-GIS performs well for both crops.

4.6. Irrigated corn yield during drought years

The result of the integrated modeling framework depicts a wide spectrum of yield change under irrigation relative to the rainfed yield at MRB during drought years. The irrigated corn yield is noted to change from 10% to 259% with the highest yields observed for 100% irrigation of IWR in the year 2012 (Fig. 10(k)). On the contrary, the lowest increase in corn yields (10 – 29%) is noted for the 50% irrigation of IWR, particularly in the western region (Mississippi) and northern region of the years 2008 and 2011 respectively. This potential low increase in yields is obvious pertaining to the unmet crop water demand during droughts even under irrigated conditions. Although, the eastern region

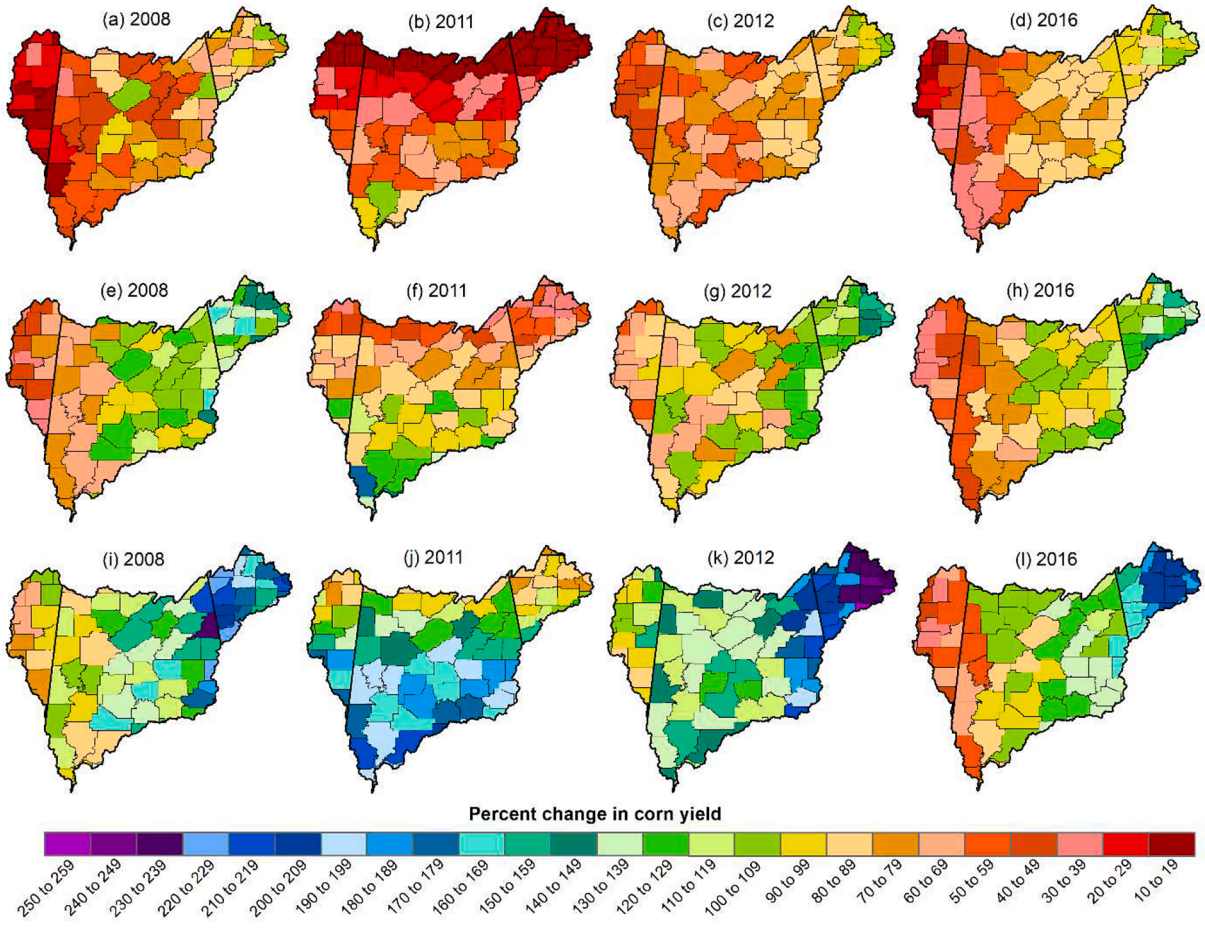

Fig. 10. Percent change in corn yield under irrigated conditions relative of rainfed corn yield at 50% of IWR for the years (a) 2008, (b) 2011, (c) 2012, and (d) 2016; 75% of IWR for the years (e) 2008, (f) 2011, (g) 2012, and (h) 2016); and 100% of IWR for the years (i) 2008, (j) 2011, (k) 2012, and (l) 2016 simulated by integrated CROPWAT-AquaCrop-GIS modeling framework. Note: The average rainfed corn yield for whole MRB is 7.70 t/ha.

(Georgia) of the basin experienced severe to extreme droughts in the year 2012, a higher increase in the corn yield (70 – 109%) is observed under 50% irrigation for the corresponding region relative to the central (Alabama) and western (Mississippi) regions (Fig. 10(c)).

In the case of 75% irrigation of IWR, a hike in the simulated yield is observed relative to the 50% irrigation for all counties irrespective of the drought years. Overall the increase in corn yield ranges from ~50% to 179% for all four drought years. A majority of the counties are noted to have a yield increase within the range of 100–159% for the year 2012 (Fig. 10(g)). This pattern of potential yield increase is consistent with that of the 50% irrigation of IWR for the eastern counties which experienced severe to extreme droughts for the year 2012. In case of the year 2016, the western counties (including Alabama and Mississippi) experienced a yield increase of 20 – 79%, whereas, the central (Alabama) and eastern (Georgia and Tennessee) counties observed to have an increase in yield within the range of 120 – 179%. This potential low yield increase in the western counties can be attributed to the near-normal precipitation conditions in the region in 2016 reflecting that IWR is met by the precipitation. On the other hand, for the eastern counties, persistent drought during the cropping period resulted in unmet IWR, which is supplemented by 75% irrigation resulting in a higher yield increase.

The corn yield simulated for 100% irrigation of IWR illustrates that the yield increase ranges from 70 to 239%, 70 to 219%, 80 to 259%, and 30 to 209% for the years 2008, 2011, 2012, and 2016 respectively across all the counties relative to the rainfed corn yield (Fig. 10(i, j, k and l)). The maximum and minimum yield increases are observed for the years 2012 and 2016, which corresponds to the highest and lowest drought intensities respectively. Interestingly for three out of four years (2008, 2012, and 2016), the peak increase in irrigated corn yield is observed for the eastern region (state of Georgia). Nevertheless, compared to all three irrigation water application rates, 100% irrigation results in the maximum potential increase in corn yield relative to the rainfed corn yield for all drought years.

4.7. Irrigated soybean yield during drought years

The irrigated soybean yield results of the integrated CROPWAT-AquaCrop-GIS modeling framework illustrates an increase in potential yield relative to the rainfed soybean yield for all counties under all three irrigation water application rates. The yield increase ranges from 20% to 229% throughout all counties under all three irrigation water application rates for all four drought years (Fig. 11). For 50% irrigation water application of IWR, the lowest potential increase in yield is noted for the year 2008 with a magnitude of 20 to 79% in the counties of central (Alabama) and western (Mississippi) region. However, the soybean yield increase is higher (90 – 119%) for the eastern region counties (Georgia). Similar results are also noted for the potential yield increase in the case of the year 2012. While for 2011, counties in the middle and the northern region are observed to have a lower magnitude of the potential yield increase relative to the southern region, the potential increase in yield is noted to range from 80% to 129% for central to eastern counties and 20% to 49% for western counties.

In the case of 75% of irrigation water application rate of IWR, the potential increase in soybean yield ranges from 50% to 189% across all counties and all four years. An analogous pattern of increase in yield is noted for the years 2008 and 2012, where the eastern counties are observed to have the highest potential increase in yield relative to the

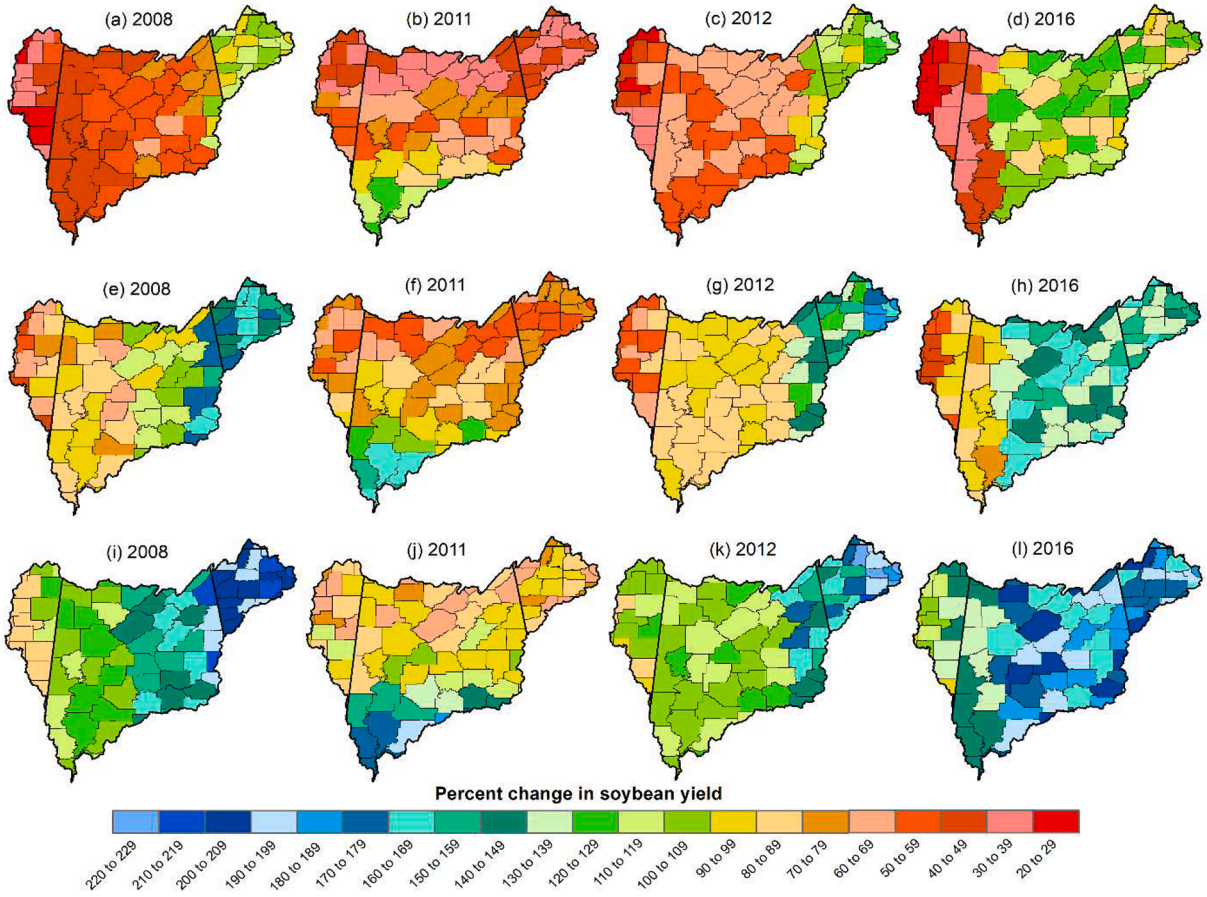

Fig. 11. Percent change in soybean yield under irrigated conditions relative of rainfed soybean yield at 50% of IWR for the years (a) 2008, (b) 2011, (c) 2012, and (d) 2016; 75% of IWR for the years (e) 2008, (f) 2011, (g) 2012, and (h) 2016); and 100% of IWR for the years (i) 2008, (j) 2011, (k) 2012, and (l) 2016 simulated by integrated CROPWAT-AquaCrop-GIS modeling framework. Note: The average rainfed soybean yield for whole MRB is 2.20 t/ha.

central and western counties (Fig. 11(e and g)). The yield increase in the case of 2016 ranges from 130% to 169% in central (Alabama state) and eastern (Georgia state) counties, whereas, 50% to 99% in western counties (Mississippi state).

Similar to the results of irrigated corn yield, the maximum potential increase in yield is observed for the 100% irrigation of IWR for all years. In Georgia and Tennessee states, the yield increase ranges from 190% to 219% relative to rainfed yield in 2008. A relatively lower increase in yield is observed for Alabama state (100 – 169%), followed by Mississippi (80 – 129%) for the corresponding year. The southern counties are observed to have the highest potential increase in soybean yield for the year 2011 (Fig. 11(j)). A relatively low range of potential soybean yield increase (100 – 139%) is observed for a majority of the counties in the year 2012, except for the eastern counties in Alabama and Georgia where the range is observed to be 140 – 229% for the corresponding year. Most of the counties in 2016 are noticed to have irrigated soybean yield in the range of 130% to 219% in Alabama, Georgia, and Tennessee states, whereas, the yield increase is merely 100% to 139% in Mississippi state (Fig. 11(l)).

5. Discussion

Droughts negatively impact crop yields by affecting the critical growth stages (Deb et al., 2015; McNider et al., 2015; Yu et al., 2018). In this study, first, county-scale agricultural drought was identified and the results indicate a majority of the counties are impacted by droughts during the years 2008, 2011, 2012, and 2016, with the most severe drought during 2012. This finding is consistent with the US drought monitor (Svoboda et al., 2002), and the SPESMI approach findings by Xu et al. (2020). By visual comparison of the drought severity derived from the SPESMI (Fig. 4) and rainfed corn and soybean yields (Figs. 5 and 6), it can be clearly seen that the yield is a response to drought severity, with lower yields noted for counties under severe to extreme droughts. Although in this study the effect of drought intensity/severity at different stages of the crop life cycle is not investigated, it would be interesting to further evaluate this in a future study.

A positive relationship between detrended crop yield and SPESMI (agricultural drought index) is found among all counties within the MRB. A positive correlation means a higher magnitude of the drought index (higher negative value; representing intense drought) leading to a poor crop yield. Although a low-intensity drought does not always guarantee a higher yield, the study region has also experienced several low intensity and frequent flash droughts (ranging from weeks to two months) in the past (Christian et al., 2019; Mo and Lettenmaier, 2020), where the crop growth can be significantly reduced, if droughts occur during the critical crop growth stages. While this analysis considered 3-month SPESMI, the effects of short-term droughts in crop yields are not accounted for, since this is beyond the scope of this paper. Nevertheless, a similar positive correlation among drought indices and crop yields was also reported by Peña-Gallardo et al. (2019) and Zhou et al. (2020) for different crops in the major cropping belts over the CONUS. Another significant finding of the correlation test is that higher correlation coefficient is noted for the state of Alabama in case of soybean crop (Fig. 7). The underlying cause for this is most likely due to the choice of soybean cultivar: Asgrow 46X6. Although this cultivar is a high yielding indeterminate variety (new leaves grow even after flowering), the cultivar is drought intolerant (Ross, 2019), since its high photosynthesis demand provokes high water stress during droughts, leading to early plant death. On the other hand, farmers of Georgia, Tennessee, and Mississippi choose a drought-resistant cultivar "USDA-N8002" over other traditional cultivars (Carter et al., 2016) which exhibits delayed canopy wilting even under drought stress leading to higher yield relative to Asgrow 46X6 cultivar.

As mentioned earlier, the novel part of this study is integrating an IWR model and a spatial crop yield simulation model in the robust estimation of crop yields during drought years while accounting for the simulated IWR/irrigation scheduling within the framework. The initial step requires, stand-alone calibration of both models, and the results of model performance are presented in Figs. S1 and S2 (supporting information file); and calibration parameters are presented in Figs. 8 and 9. It is worth noting that the poor CROPWAT model performance during validation for corn in the eastern counties is likely due to the underestimation of the plant available water by the model, particularly in Georgia. This is because Georgia has the highest number of farmland in the region leading to a significant amount of soil preparation (tillage) and since the model employs the USDA soil conservation service approach of effective rainfall calculation (which is empirical), the model likely fails in the robust calculation of the water loss leading to inaccurate estimation of plant available water. Similar poor CROPWAT model performance in agriculture dominant regions were also reported by Awad et al. (2021) and Babu et al. (2015). Overall, these results indicate both models are in good agreement with the observed/reported variables across all counties.

While the overall area under irrigation in the US continues to rise, specifically in the major corn and soybean belts, rainfed agricultural practices are dominant in the deep southern states (Portmann et al., 2010). The results of this study indicate that IWR varies spatially and temporally at MRB. For instance, IWR ranges from 80 to 319 mm and 60 to 419 mm during the years 2008 and 2012 respectively for corn (Fig. S6 (a and c)). Similarly, IWR varies between 0 and 259 mm and 40 to 419 mm for the corresponding years respectively in the case of soybean (Fig. S7(a and c)). This illustrates that a significant amount of water required by crops is unmet by precipitation during drought years. Another critical finding of the IWR simulation is that the severe to extreme drought-impacted counties show higher IWR. This is apparent since during droughts vapor pressure deficit is higher relative to the normal precipitation period and this results in higher transpiration from crops (Luo et al., 2016). Although, it is also argued that during water stress, crops either roll up or reduce intake of sunlight to reduce photosynthesis and thus the lowering water requirement; however, crop transpiration does not significantly reduce until the soil moisture falls below 50% of the available water capacity (Schneekloth and Andales, 2017). Nevertheless, this study indicates that the IWR is higher in the counties experiencing severe to extreme droughts.

The simulation of the integrated framework illustrates the maximum yield can be potentially achieved at the counties which experience the most intense droughts. This is obvious since supplemental irrigation eliminates plant water stress (Fereres and Soriano, 2007). It is noteworthy that during intense droughts, higher temperature leads to increased plant water use and this contributes to high plant mortality rate/reduced yield since water is unavailable during droughts under rainfed agriculture (Will et al., 2013). Another important finding of the integrated modeling framework is that the maximum yield can be attained by 100% irrigation of IWR in the most intense drought-affected counties for both crops (Figs. 10 and 11). These findings highlight that in order to meet the water demands of increasing the corn and soybean yields, irrigation is imperative and hence a change in the current agricultural practices is crucial to combat these negative impacts of droughts and make the region more self-reliant. Moreover, given the projected scarcity of water in the future, judicious use of water is critical and integrated modeling approaches such as one suggested here can play a decisive role in increasing crop yield under droughts relative to the concurrent practices.

While global gridded crop models are also available in literature which can be forced with IWR datasets, due to their coarse spatial resolution (grid size often >70 km), the results are unreliable and are not applicable for regional to county-scale irrigation water planning and management. Moreover, these models require high performance computing and high-level coding skills. Whereas, the integrated modeling framework employed here is widely applicable for regional-scale studies and does not require high coding expertise, and can be used by a water modeler for simulating robust county-scale agricultural

plans under droughts. The authors acknowledge that a limitation of this study is lumping the spatial soil characteristics at county-scale in the integrated modeling framework. However, this study intends to demonstrate the applicability of the novel framework at county-scale for better agricultural planning and management under drought conditions in rainfed dominant regions. Of course, with the availability of finer spatial information (farm-scale or micro-basin scale crop yield, weather dataset, and soil information) the outputs of the integrated modeling framework can be of further help for micro-basin scale agricultural management. It is also critical to note that although more irrigation water requires higher monetary investment (including water cost, installation, and maintenance of the irrigation system), analyzing this and identifying the optimal irrigation water application rate while accounting for the irrigation costs is beyond the scope of this paper.

A plethora of studies have coupled crop models with hydrological (both surface water and groundwater) and irrigation models in the past (e.g. McNider et al., 2015; Mcnider et al., 2011; Lopez et al., 2017; Rossetto et al., 2019; Roy et al., 2019; Sabzzadeh & Shourian, 2020). While these studies are conducted with the primary objective of optimization of irrigation using subsurface water retention technology, developing irrigation scheduling in a crop model, and simulating conjunctive use of irrigation water resources, none has applied a multi-model integration framework in simulation of maximizing the potential crop yields using irrigation under droughts. Moreover, although AquaCrop (the core component of the AquaCrop-GIS model) is a widely used model globally, the application of the spatial version of the model i.e., AquaCrop-GIS model employed in this study is limited, therefore, this study further reinforces the latter's applicability at the basin-scale. Furthermore, the model integration framework proposed in this study is simple and provides the flexibility of model selection (since models used in this framework can be replaced by other models) over other published studies. Hence, it is a versatile framework and its further application is suggested at a continental/country scale for robust irrigation planning and management.

6. Conclusion

While crop yields under rainfed cultivation practices generally decline during droughts, irrigation can play a critical role in reducing crop yield loss. However, given the constraint of water scarcity during droughts, an accurate estimation of the IWR and irrigation scheduling is critical. Therefore, this study presents a novel integrated modeling framework by using two parsimonious models namely, CROPWAT (an IWR simulation model) and AquaCrop-GIS (a spatial crop yield simulation model) to simulate corn and soybean yields at county-scale under droughts in the MRB. The calculation of SPESMI (agricultural drought index) suggests mild to severe droughts varying spatially across the counties during the years 2008, 2011, 2012, and 2016. Additionally, a moderate to strong positive correlation is also noted among SPESMI and detrended crop yields across the counties. Furthermore, the integrated modeling approach reveals an increase in corn and soybean yields ranging from 10% to 259% and 20% to 229% respectively under different irrigation water application rates relative to rainfed crop yield for the four drought years within MRB.

Although the integrated modeling framework presented in this study is time-consuming, it is essential in the Deep South region and other similar regions where droughts are frequent and recurrent, and farmers generally practice rainfed agriculture (Craig et al., 2019). The integrated modeling framework simulates IWR and crop yield robustly and helps in devising better irrigation planning and management under drought conditions. This is because the integrated modeling framework is capable of intaking the current operational weather prediction as input in calculating appropriate IWR and resulting potential increase in the crop yields, especially during forecasted droughts. Furthermore, the findings of this study can be used by state or local governments for capacity building and educating farmers to transition from rainfed to irrigated agriculture to avoid crop yield loss in the future. It is worth noting that shifting from rainfed to irrigated agriculture may consume the regional surface or groundwater resources. While some regions may be water–limited and are not capable to attain the 100% irrigation level, the irrigation should be based on water availability. Although the aim of this paper is not to evaluate how much water is realistically available for irrigation during droughts or whether is it economically viable, the authors plan to investigate these questions in their future research.

Declaration of Competing Interest

The authors declare that they have no known competing financial interests or personal relationships that could have appeared to influence the work reported in this paper.

Acknowledgement

Financial support was provided by the National Science Foundation, Grant 1856054.

Appendix A. Supplementary data

Supplementary data to this article can be found online at https://doi.org/10.1016/j.jhydrol.2022.127760.

References

Abbaszadeh, P., Moradkhani, H., Zhan, X., 2019. Downscaling SMAP Radiometer Soil Moisture Over the CONUS Using an Ensemble Learning Method. Water Resour. Res. 55, 324–344. https://doi.org/10.1029/2018WR023354.

Abbaszadeh, Peyman, Moradkhani, Hamid, Gavahi, Keyhan, Kumar, Sujay, Hain, Christopher, Zhan, Xiwu, Duan, Qingyun, Peters-Lidard, Christa, Karimiziarani, Sepehr, 2021. High-resolution SMAP satellite soil moisture product: exploring the opportunities. Bulletin of the American Meteorological Society 309–315. https://doi.org/10.1175/BAMS-D-21-0016.1. In press.

Abbaszadeh, Peyman, Gavahi, Keyhan, Alipour, Atieh, Deb, Proloy, Moradkhani, Hamid, 2022. Bayesian Multi-modeling of Deep Neural Nets for Probabilistic Crop Yield Prediction. Agricultural and Forest Meteorology 314, 108773. https://doi.org/10.1016/j.agrformet.2021.108773. In press.

Alderman, P.D., 2021. Parallel gridded simulation framework for DSSAT-CSM (version 4.7.5.21) using MPI and NetCDF. Geosci. Model Dev. 14, 6541–6569. https://doi.org/10.5194/GMD-14-6541-2021.

Alexandratos, N., Bruinsma, J., 2012. World Agriculture towards 2030/2050: the 2012 revision. WORLD AGRICULTURE, Rome.

Allen, R., Pereira, L., Raes, D., Smith, M., 1998. Crop Evapotranspiration: Guidelines for Computing Crop Water Requirements. Italy, Rome.

Awad, A., Wan, L., El-Rawy, M., Eltarabily, M.G., 2021. Proper predictions of the water fate in agricultural lands: Indispensable condition for better crop water requirements estimates. Ain Shams Eng. J. 12, 2435–2442. https://doi.org/10.1016/J.ASEJ.2021.02.003.

Babel, M.S., Deb, P., Soni, P., 2019. Performance Evaluation of AquaCrop and DSSAT-CERES for Maize Under Different Irrigation and Manure Application Rates in the Himalayan Region of India. Agric. Res. 8, 207–217. https://doi.org/10.1007/s40003-018-0366-y.

Babu, R.G., Babu, G.R., Kumar, H.V.H., 2015. Estimation of crop water requirement, effective rainfall and irrigation water requirement for vegetable crops using CROPWAT. Int. J. Agric. Eng. 8 (1), 15–20.

Balkcom, K., Brooke, A., Burmester, C.H., Conner, K., Delaney, D., Delaney, M., Griffith, W., Hall, M., Howe, J., Hicks, C., Huluka, G., Lawrence, K.S., Mask, P.L., 2014. Auburn University of Crops: Soybean Research Report 2013 & 2014. Auburn.

Boretti, A., Rosa, L., 2019. Reassessing the projections of the World Water Development Report. npj Clean. Water 2, 1–6. https://doi.org/10.1038/s41545-019-0039-9.

Carrão, H., Russo, S., Sepulcre-Canto, G., Barbosa, P., 2016. An empirical standardized soil moisture index for agricultural drought assessment from remotely sensed data. Int. J. Appl. Earth Obs. Geoinf. 48, 74–84. https://doi.org/10.1016/j.jag.2015.06.011.

Carter, T.E., Todd, S.M., Gillen, A.M., 2016. Registration of 'USDA-N8002' Soybean Cultivar with High Yield and Abiotic Stress Resistance Traits. J. Plant Regist. 10 (3), 238–245.

Christian, J.I., Basara, J.B., Otkin, J.A., Hunt, E.D., 2019. Regional characteristics of flash droughts across the United States. Environ. Res. Commun. 1 (12), 125004.

Craig, C.A., Feng, S., Gilbertz, S., 2019. Water crisis, drought, and climate change in the southeast United States. Land use policy 88, 104110. https://doi.org/10.1016/j.landusepol.2019.104110.

Dai, Y., Xin, Q., Wei, N., Zhang, Y., Shangguan, W., Yuan, H., Zhang, S., Liu, S., Lu, X., 2019. A Global High-Resolution Data Set of Soil Hydraulic and Thermal Properties for Land Surface Modeling. J. Adv. Model. Earth Syst. 11, 2996–3023. https://doi.org/10.1029/2019MS001784.

Deb, P., Debnath, P., Denis, A.F., Lepcha, O.T., 2019. Variability of soil physicochemical properties at different agroecological zones of Himalayan region: Sikkim. India. Environ. Dev. Sustain. 21 (5), 2321–2339.
Deb, P., Kiem, A.S., 2020. Evaluation of rainfall–runoff model performance under non-stationary hydroclimatic conditions. Hydrol. Sci. J. 65, 1667–1684. https://doi.org/10.1080/02626667.2020.1754420.
Deb, P., Shrestha, S., Babel, M.S., 2015. Forecasting climate change impacts and evaluation of adaptation options for maize cropping in the hilly terrain of Himalayas: Sikkim. India. Theor. Appl. Climatol. 121, 649–667. https://doi.org/10.1007/s00704-014-1262-4.
Duan, Q., Sorooshian, S., Gupta, V.K., 1994. Optimal use of the SCE-UA global optimization method for calibrating watershed models. J. Hydrol. 158, 265–284. https://doi.org/10.1016/0022-1694(94)90057-4.
Duan, Q.Y., Gupta, V.K., Sorooshian, S., 1993. Shuffled complex evolution approach for effective and efficient global minimization. J. Optim. Theory Appl. 76, 501–521. https://doi.org/10.1007/BF00939380.
Duzy, L.M., Price, A.J., Balkcom, K.S., Aulakh, J.S., 2016. Assessing the Economic Impact of Inversion Tillage, Cover Crops, and Herbicide Regimes in Palmer Amaranth (Amaranthus palmeri) Infested Cotton. Int. J. Agron. 2016, 1–9.
Edwards, G., Walker, D., 1983. C3, C4: mechanisms, and cellular and environmental regulation of photosynthesis. Blackwell Scientific Publications, Oxford.
Evans, R.G., Sadler, E.J., 2008. Methods and technologies to improve efficiency of water use. Water Resour. Res. 44 https://doi.org/10.1029/2007WR006200.
Fao, 2017. Book I. Understanding AquaCrop, Rome.
Fao CROPWAT: A computer program for irrigation planning and management 1992 Rome.
Fereres, E., Soriano, M.A., 2007. Deficit irrigation for reducing agricultural water use, in. Journal of Experimental Botany. Oxford Academic 147–159. https://doi.org/10.1093/jxb/erl165.
Foley, J.A., Ramankutty, N., Brauman, K.A., Cassidy, E.S., Gerber, J.S., Johnston, M., Mueller, N.D., O'Connell, C., Ray, D.K., West, P.C., Balzer, C., Bennett, E.M., Carpenter, S.R., Hill, J., Monfreda, C., Polasky, S., Rockström, J., Sheehan, J., Siebert, S., Tilman, D., Zaks, D.P.M., 2011. Solutions for a cultivated planet. Nature 478, 337–342. https://doi.org/10.1038/nature10452.
Fraisse, C.W., Breuer, N.E., Zierden, D., Bellow, J.G., Paz, J., Cabrera, V.E., Garcia y Garcia, A., Ingram, K.T., Hatch, U., Hoogenboom, G., Jones, J.W., O'Brien, J.J., 2006. AgClimate: A climate forecast information system for agricultural risk management in the southeastern USA. Comput. Electron. Agric. 53 (1), 13–27.
Gavahi, K., Abbaszadeh, P., Moradkhani, H., Zhan, X., Hain, C., 2020. Multivariate assimilation of remotely sensed soil moisture and evapotranspiration for drought monitoring. J. Hydrometeorol. 21, 2293–2308. https://doi.org/10.1175/JHM-D-20-0057.1.
Gavahi, Keyhan, Abbaszadeh, Peyman, Moradkhani, Hamid, 2021. DeepYield: A combined convolutional neural network with long short-term memory for crop yield forecasting. Expert Systems with Applications 184, 115511. https://doi.org/10.1016/j.eswa.2021.115511. In press.
Geerts, S., Raes, D., Garcia, M., Miranda, R., Cusicanqui, J.A., Taboada, C., Mendoza, J., Huanca, R., Mamani, A., Condori, O., Mamani, J., Morales, B., Osco, V., Steduto, P., 2009. Simulating Yield Response of Quinoa to Water Availability with AquaCrop. Agron. J. 101, 499–508. https://doi.org/10.2134/agronj2008.0137s.
Glass, K.M., Delaney, D., Monks, C.D., Brasher, J., 2018. Performance of soybean cultivars in Alabama, 2018. Auburn, AL.
Glass, K.M., Delaney, D.P., Monks, C.D., Brasher, J., 2016. Performance of field corn hybrids in Alabama, 2016. Auburn, AL.
Hameed, M., Ahmadalipour, A., Moradkhani, H., 2020. Drought and food security in the middle east: An analytical framework. Agric. For. Meteorol. 281, 107816 https://doi.org/10.1016/j.agrformet.2019.107816.
Harvey, A., Trimbur, T., 2008. Trend estimation and the Hodrick-Prescott filter. J. Japan Stat. Soc. 38 (1), 41–49.
P. Hollis Obstacles still hinder irrigation in Alabama | Farm Progress [WWW Document] Southeast FarmPress. 2011 accessed 3.3.22 https://www.farmprogress.com/equipment/obstacles-still-hinder-irrigation-alabama.
Jones, J.W., Hoogenboom, G., Porter, C.H., Boote, K.J., Batchelor, W.D., Hunt, L.A., Wilkens, P.W., Singh, U., Gijsman, A.J., Ritchie, J.T., 2003. The DSSAT cropping system model. Eur. J. Agron. 18, 235–265. https://doi.org/10.1016/S1161-0301(02)00107-7.
Kephe, P.N., Ayisi, K.K., Petja, B.M., 2021. Challenges and opportunities in crop simulation modelling under seasonal and projected climate change scenarios for crop production in South Africa. Agric & Food Secur 10 (1).
Kim, K.-H., Doi, Y., Ramankutty, N., Iizumi, T., 2021. A review of global gridded cropping system data products. Environ. Res. Lett. 16 (9), 093005.
Kim, W., Iizumi, T., Nishimori, M., 2019. Global patterns of crop production losses associated with droughts from 1983 to 2009. J. Appl. Meteorol. Climatol. 58, 1233–1244. https://doi.org/10.1175/JAMC-D-18-0174.1.
M.V. Lara C.S. Andreo C4 Plants Adaptation to High Levels of CO2 and to Drought Environments A. Shanker B. Venkateswarlu Abiotic Stress in Plants – Mechanisms and Adaptations 2011 IntechOpen, London, UK 415 428 10.5772/24936.
Lesk, C., Rowhani, P., Ramankutty, N., 2016. Influence of extreme weather disasters on global crop production. Nature 529, 84–87. https://doi.org/10.1038/nature16467.
Lokupitiya, R.S., Lokupitiya, E., Paustian, K., 2006. Comparison of missing value imputation methods for crop yield data. Environmetrics 17, 339–349. https://doi.org/10.1002/env.773.
Lopez, J.R., Winter, J.M., Elliott, J., Ruane, A.C., Porter, C., Hoogenboom, G., 2017. Integrating growth stage deficit irrigation into a process based crop model. Agric. For. Meteorol. 243, 84–92. https://doi.org/10.1016/j.agrformet.2017.05.001.
Lu, J., Carbone, G.J., Gao, P., 2017. Detrending crop yield data for spatial visualization of drought impacts in the United States, 1895–2014. Agric. For. Meteorol. 237–238, 196–208. https://doi.org/10.1016/J.AGRFORMET.2017.02.001.
Luo, Z., Guan, H., Zhang, X., Zhang, C., Liu, N., Li, G., 2016. Responses of plant water use to a severe summer drought for two subtropical tree species in the central southern China. J. Hydrol. Reg. Stud. 8, 1–9. https://doi.org/10.1016/j.ejrh.2016.08.001.
Madadgar, S., Moradkhani, H., 2013. A Bayesian framework for probabilistic seasonal drought forecasting. J. Hydrometeorol. 14, 1685–1705. https://doi.org/10.1175/JHM-D-13-010.1.
Masud, M.B., Khaliq, M.N., Wheater, H.S., 2015. Analysis of meteorological droughts for the Saskatchewan River Basin using univariate and bivariate approaches. J. Hydrol. 522, 452–466. https://doi.org/10.1016/j.jhydrol.2014.12.058.
McDonald, R.I., Girvetz, E.H., Ibekwe, A.M., 2013. Two Challenges for U.S. Irrigation Due to Climate Change: Increasing Irrigated Area in Wet States and Increasing Irrigation Rates in Dry States. PLoS One 8 (6), e65589.
McKee, T., Doeskin, N., Kleist, J., 1993. The relationship of drought frequency and duration to time scales. In: 8th Conference on Applied Climatology. American Meteorological Society, Anaheim, Canada, pp. 179–184.
Mcnider, R.T., Christy, J.R., Moss, D., Doty, K., Handyside, C., Limaye, A., Garcia, A.G.Y., Hoogenboom, G., 2011. A real-time gridded crop model for assessing spatial drought stress on crops in the Southeastern United States. J. Appl. Meteorol. Climatol. 50, 1459–1475. https://doi.org/10.1175/2011JAMC2476.1.
McNider, R.T., Handyside, C., Doty, K., Ellenburg, W.L., Cruise, J.F., Christy, J.R., Moss, D., Sharda, V., Hoogenboom, G., Caldwell, P., 2015. An integrated crop and hydrologic modeling system to estimate hydrologic impacts of crop irrigation demands. Environ. Model. Softw. 72, 341–355. https://doi.org/10.1016/j.envsoft.2014.10.009.
Mitchell, K.E., Lohmann, D., Houser, P.R., Wood, E.F., Schaake, J.C., Robock, A., Cosgrove, B.A., Sheffield, J., Duan, Q., Luo, L., Higgins, R.W., Pinker, R.T., Tarpley, J.D., Lettenmaier, D.P., Marshall, C.H., Entin, J.K., Pan, M., Shi, W., Koren, V., Meng, J., Ramsay, B.H., Bailey, A.A., 2004. The multi-institution North American Land Data Assimilation System (NLDAS): Utilizing multiple GCIP products and partners in a continental distributed hydrological modeling system. J. Geophys. Res. Atmos. 109 https://doi.org/10.1029/2003JD003823.
Mo, K.C., Lettenmaier, D.P., 2020. Prediction of flash droughts over the united states. J. Hydrometeorol. 21, 1793–1810. https://doi.org/10.1175/JHM-D-19-0221.1.
Molnar, J.J., Sydnor, E., Rodekohr, D., Runge, M., Fowler, S., 2011. Farm operator percentions of barriers to the use of irrigation in Alabama. Alabama Agric. Exp. Stn. 1–24.
E.M. Molter W.D. Collins M.D. Risser Quantitative Precipitation Estimation of Extremes in CONUS With Radar Data Geophys. Res. Lett. 48 2021 e2021GL094697 10.1029/2021GL094697.
D.N. Moriasi J.G. Arnold M.W. Van Liew R.L. Bingner R.D. Harmel T.L. Veith Model evaluation guidelines for systematic quantification of accuracy in watershed simulations Trans. ASABE 50 2007 885 900 https://doi.org/10.13031/2013.23153.
Mubeen, M., Ahmad, A., Hammad, H.M., Awais, M., Farid, H.U., Saleem, M., Din, M.S.u., Amin, A., Ali, A., Fahad, S., Nasim, W., 2020. Evaluating the climate change impact on water use efficiency of cotton-wheat in semi-arid conditions using DSSAT model. J. Water Clim. Chang. 11 (4), 1661–1675.
Müller, C., Elliott, J., Kelly, D., Arneth, A., Balkovic, J., Ciais, P., Deryng, D., Folberth, C., Hoek, S., Izaurralde, R.C., Jones, C.D., Khabarov, N., Lawrence, P., Liu, W., Olin, S., Pugh, T.A.M., Reddy, A., Rosenzweig, C., Ruane, A.C., Sakurai, G., Schmid, E., Skalsky, R., Wang, X., de Wit, A., Yang, H., 2019. The Global Gridded Crop Model Intercomparison phase 1 simulation dataset. Sci Data 6 (1).
Nelder, J.A., Mead, R., 1965. A simplex method for function minimization. Comput. J. 7 (4), 308–313.
Novak, J.L., Nadolnyak, D., McNider, R., 2008. Analysis of irrigated corn production adoption decisions in Alabama, in: 2008 Annual Meetings of the SAEA. Southern Agricultural Economics Association, Dallas, TX.
Nrcs A statistical survey of land use and natural resource conditions and trends on U.S. non-Federal lands [WWW Document] U.S. Dep. Agric. Nat. Resour. Conserv. Serv. 2017 accessed 3.4.22 https://www.nrcs.usda.gov/wps/portal/nrcs/main/national/technical/nra/nri/.
Park, S., Im, J., Jang, E., Rhee, J., 2016. Drought assessment and monitoring through blending of multi-sensor indices using machine learning approaches for different climate regions. Agric. For. Meteorol. 216, 157–169. https://doi.org/10.1016/j.agrformet.2015.10.011.
Peña-Gallardo, M., Vicente-Serrano, S.M., Quiring, S., Svoboda, M., Hannaford, J., Tomas-Burguera, M., Martín-Hernández, N., Domínguez-Castro, F., El Kenawy, A., 2019. Response of crop yield to different time-scales of drought in the United States: Spatio-temporal patterns and climatic and environmental drivers. Agric. For. Meteorol. 264, 40–55. https://doi.org/10.1016/j.agrformet.2018.09.019.
F.T. Portmann S. Siebert P. Döll MIRCA2000-Global monthly irrigated and rainfed crop areas around the year 2000: A new high-resolution data set for agricultural and hydrological modeling Global Biogeochem. Cycles 24 1 2010 n/a n/a.
Puy, A., Lo Piano, S., Saltelli, A., 2020. Current Models Underestimate Future Irrigated Areas. Geophys. Res. Lett. 47 https://doi.org/10.1029/2020GL087360.
Quiring, S.M., Papakryiakou, T.N., 2003. An evaluation of agricultural drought indices for the Canadian prairies. Agric. For. Meteorol. 118, 49–62. https://doi.org/10.1016/S0168-1923(03)00072-8.
Ray, R.L., Fares, A., Risch, E., 2018. Effects of Drought on Crop Production and Cropping Areas in Texas. Agric. Environ. Lett. 3 (1), 170037.
Ross, J., 2019. Arkansas Soybean Research Studies 2018. Fayetteville, Arkansas.
Rossetto, R., De Filippis, G., Triana, F., Ghetta, M., Borsi, I., Schmid, W., 2019. Software tools for management of conjunctive use of surface- and ground-water in the rural environment: integration of the Farm Process and the Crop Growth Module in the

FREEWAT platform. Agric. Water Manag. 223, 105717 https://doi.org/10.1016/j.agwat.2019.105717.
Roy, P.C., Guber, A., Abouali, M., Nejadhashemi, A.P., Deb, K., Smucker, A.J.M., 2019. Crop yield simulation optimization using precision irrigation and subsurface water retention technology. Environ. Model. Softw. 119, 433–444. https://doi.org/10.1016/j.envsoft.2019.07.006.
Rubin, D.B., 1987. Multiple Imputation for Nonresponse in Surveys. Wiley, New York.
Sabzzadeh, I., Shourian, M., 2020. Maximizing crops yield net benefit in a groundwater-irrigated plain constrained to aquifer stable depletion using a coupled PSO-SWAT-MODFLOW hydro-agronomic model. J. Clean. Prod. 262, 121349 https://doi.org/10.1016/j.jclepro.2020.121349.
G.D. Schaible M.P. Aillery Water conservation in irrigated agriculture: Trends and challenges in the face of emerging demands 2012 Washington DC.
Schauberger, B., Ben-Ari, T., Makowski, D., Kato, T., Kato, H., Ciais, P., 2018. Yield trends, variability and stagnation analysis of major crops in France over more than a century. Sci. Rep. 8, 1–12. https://doi.org/10.1038/s41598-018-35351-1.
J. Schneekloth A. Andales Seasonal Water Needs and Opportunities for Limited Irrigation for Colorado Crops 2017 Fort Collins CO.
Shrestha, S., Deb, P., Bui, T.T.T., 2016. Adaptation strategies for rice cultivation under climate change in Central Vietnam. Mitig. Adapt. Strateg. Glob. Chang. 21 (1), 15–37.
Shrestha, S., Thin, N.M.M., Deb, P., 2014. Assessment of climate change impacts on irrigation water requirement and rice yield for Ngamoeyeik irrigation project in Myanmar. J. Water Clim. Chang. 5, 427–442. https://doi.org/10.2166/wcc.2014.114.
Siebert, S., Döll, P., 2010. Quantifying blue and green virtual water contents in global crop production as well as potential production losses without irrigation. J. Hydrol. 384, 198–217. https://doi.org/10.1016/j.jhydrol.2009.07.031.
M. Smith CROPWAT : a Computer Program for Irrigation Planning and Management 1992 Rome.
Steduto, P., Hsiao, T.C., Raes, D., Fereres, E., 2009. AquaCrop-The FAO Crop Model to Simulate Yield Response to Water: I. Concepts and Underlying Principles. Agron. J. 101, 426–437. https://doi.org/10.2134/agronj2008.0139s.
Sun, G., Arumugam, S., Caldwell, P.V., Conrads, P.A., Covich, A.P., Cruise, J., Feldt, J., Georgakakos, A.P., McNider, R.T., McNulty, S.G., Marion, D.A., Misra, V., Rasmussen, T.C., Romolo, L., Terando, A., 2013. Impacts of climate change and variability on water resources in the Southeast USA. In: Climate of the Southeast United States: Variability. and Vulnerability. Island Press-Center for Resource Economics, Change, Impacts, pp. 210–236. https://doi.org/10.5822/978-1-61091-509-0_10.
Svoboda, M., LeComte, D., Hayes, M., Heim, R., Gleason, K., Angel, J., Rippey, B., Tinker, R., Palecki, M., Stooksbury, D., Miskus, D., Stephens, S., 2002. The Drought Monitor. Bull. Am. Meteorol. Soc. 83, 1181–1190. https://doi.org/10.1175/1520-0477-83.8.1181.
G.Y. Tsuji G. Hoogenboom P.K. Thornton Understanding Options for Agricultural Production 1998 Springer, Netherlands, Dordrecht Systems Approaches for Sustainable Agricultural Development 10.1007/978-94-017-3624-4.
Uniyal, B., Dietrich, J., Vu, N.Q., Jha, M.K., Arumí, J.L., 2019. Simulation of regional irrigation requirement with SWAT in different agro-climatic zones driven by observed climate and two reanalysis datasets. Sci. Total Environ. 649, 846–865. https://doi.org/10.1016/J.SCITOTENV.2018.08.248.
USDA, N., 1997. Usual Planting and Harvesting Dates for U.S. Field Crops. Washington D. C.
Van Loon, A.F., Gleeson, T., Clark, J., Van Dijk, A.I.J.M., Stahl, K., Hannaford, J., Di Baldassarre, G., Teuling, A.J., Tallaksen, L.M., Uijlenhoet, R., Hannah, D.M., Sheffield, J., Svoboda, M., Verbeiren, B., Wagener, T., Rangecroft, S., Wanders, N., Van Lanen, H.A.J., 2016. Drought in the Anthropocene. Nat. Geosci. 92 (9), 89–91. https://doi.org/10.1038/ngeo2646.
Warner, K.A., Bonzongo, J.C.J., Roden, E.E., Ward, G.M., Green, A.C., Chaubey, I., Lyons, W.B., Arrington, D.A., 2005. Effect of watershed parameters on mercury distribution in different environmental compartments in the Mobile Alabama River Basin, USA. Sci. Total Environ. 347, 187–207. https://doi.org/10.1016/j.scitotenv.2004.12.011.
Will, R.E., Wilson, S.M., Zou, C.B., Hennessey, T.C., 2013. Increased vapor pressure deficit due to higher temperature leads to greater transpiration and faster mortality during drought for tree seedlings common to the forest-grassland ecotone. New Phytol. 200, 366–374. https://doi.org/10.1111/nph.12321.
Woli, P., Jones, J.W., Ingram, K.T., Fraisse, C.W., 2012. Agricultural Reference Index for Drought (ARID). Agron. J. 104, 287–300. https://doi.org/10.2134/AGRONJ2011.0286.
Xia, Y., Ford, T.W., Wu, Y., Quiring, S.M., Ek, M.B., 2015. Automated quality control of in situ soil moisture from the north american soil moisture database using NLDAS-2 products. J. Appl. Meteorol. Climatol. 54, 1267–1282. https://doi.org/10.1175/JAMC-D-14-0275.1.
Xu, L., Abbaszadeh, P., Moradkhani, H., Chen, N., Zhang, X., 2020. Continental drought monitoring using satellite soil moisture, data assimilation and an integrated drought index. Remote Sens. Environ. 250, 112028 https://doi.org/10.1016/j.rse.2020.112028.
Yu, C., Huang, X., Chen, H., Huang, G., Ni, S., Wright, J.S., Hall, J., Ciais, P., Zhang, J., Xiao, Y., Sun, Z., Wang, X., Yu, L., 2018a. Assessing the Impacts of Extreme Agricultural Droughts in China Under Climate and Socioeconomic Changes. Earth's Futur. 6, 689–703. https://doi.org/10.1002/2017EF000768.
Yu, H., Zhang, Q., Sun, P., Song, C., 2018b. Impact of Droughts on Winter Wheat Yield in Different Growth Stages during 2001–2016 in Eastern China. Int. J. Disaster Risk Sci. 9, 376–391. https://doi.org/10.1007/s13753-018-0187-4.
Zhou, W., Guan, K., Peng, B., Shi, J., Jiang, C., Wardlow, B., Pan, M., Kimball, J.S., Franz, T.E., Gentine, P., He, M., Zhang, J., 2020. Connections between the hydrological cycle and crop yield in the rainfed U.S. Corn Belt. J. Hydrol. 590, 125398 https://doi.org/10.1016/j.jhydrol.2020.125398.
Zipper, S.C., Qiu, J., Kucharik, C.J., 2016. Drought effects on US maize and soybean production: spatiotemporal patterns and historical changes. Environ. Res. Lett. 11 (9), 094021.